CHAPTER 20

Methods and Applications of Site-Directed Spin Labeling EPR Spectroscopy

Candice S. Klug and Jimmy B. Feix

Department of Biophysics
Medical College of Wisconsin
Milwaukee, Wisconsin 53226

Abstract

Site-directed spin labeling (SDSL) electron paramagnetic resonance (EPR) spectroscopy has emerged as a well-established method that can provide specific information on the location and environment of an individual residue within large and complex protein structures. The SDSL technique involves introducing a cysteine residue at the site of interest and then covalently labeling with a sulfhydryl-specific spin label containing a stable free radical, which is used as the

METHODS IN CELL BIOLOGY, VOL. 84

0091-679X/08 $35.00
DOI: 10.1016/S0091-679X(07)84020-9

EPR-detectable probe. SDSL directly probes the local environment, structure, and proximity of individual residues, and is often greatly advantageous over techniques that give global information on protein structure and changes. SDSL can detect and follow changes in local structure due to intramolecular conformational changes or dynamic interactions with other proteins, peptides, or substrates. In addition, this technique can detect changes in distances between two sites and provide information on the depth of spin labels located within a membrane bilayer. EPR is neither limited by the size of the protein or peptide nor limited by the optical properties of the sample and has the unique ability to address and answer structure and dynamics questions that are not solvable solely by genetic or crystal structure analysis, making it highly complementary to other structural methods.

In this chapter, we introduce the basic methods for using SDSL EPR spectroscopy in the study of the structure and dynamics of proteins and peptides and illustrate the practical applications of this method through specific examples in the literature.

I. Background and Methods

A. The Technique

The site-directed spin labeling (SDSL) technique involves the covalent attachment of a spin label side chain, which contains a stable unpaired electron, to a specific site on a protein or peptide. The most commonly used spin label is the sulfhydryl-specific nitroxide, 2,2,5,5-tetramethyl-l-oxyl-3-methyl methanethiosulfonate (MTSL, Toronto Research Chemicals; Fig. 1). This probe contains an unpaired electron, which is localized primarily in the p_z orbital of the ^{14}N atom, and the probe is typically reacted with a cysteine residue as it is the only amino acid side chain containing a sulfhydryl group.

Because the SDSL method requires unique cysteines for site-specific introduction of the spin label, any native cysteines within a protein need to be substituted with another amino acid using polymerase chain reaction techniques or proven to be unreactive to the spin label due to disulfide bond formation or lack of

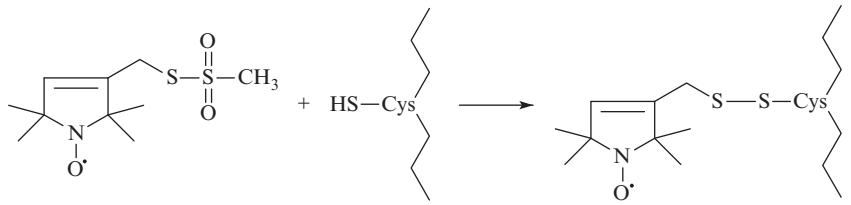

Fig. 1 Covalent attachment of the spin label to a cysteine residue. Site-specific introduction of the spin label is achieved through the selective reaction of the methanethiosulfonate group with the sulfhydryl group of the cysteine residue.

accessibility. Once the reactive cysteines have been removed, unique cysteines are introduced at each site of interest and the mutant proteins are expressed and purified. Considerable experience over the past 15 years has established that proteins are highly resilient to site-specific introduction of cysteine residues. Numerous examples now exist in the literature where a large number of sites in a given protein have been mutated to cysteine and spin labeled without loss of function (e.g., Perozo *et al*., 1998, 2002; Xu *et al*., 2005; Yang *et al*., 1996). Indeed, one of the advantages of the SDSL technique is the small size and minimal perturbation of the probe.

Spin labels are sold in powder form and are typically made into a small volume (e.g., 50–100 μl), 200 mM stock solution in 100% acetonitrile (ACN). This solution is kept at $-20\,^{\circ}$C and wrapped in foil. From this stock solution, dilutions are made for each labeling experiment and used immediately. (Once in aqueous solution, MTSL will react with itself to give a disulfide-linked dimer, reducing the concentration available for reaction with the protein or peptide. This reaction does not occur in 100% ACN.) Generally, the spin label is added at a tenfold molar excess over the purified protein concentration in a buffer of pH 6.8. In most cases, the protein will precipitate out of solution if 100% ACN is added directly to the protein solution. So, dilutions from the 200 mM stock must first be made (in the protein or labeling buffer) to bring the ACN concentration to below 10%. For example, for 1 ml of 20 μM purified protein, add 1 μl of the 200 mM stock solution to 10–100 μl of buffer and then add the entire dilution volume to the protein solution. This will give a tenfold excess of spin label and keep the ACN concentration added to the protein solution at or below 10%. This is gently mixed on a nutator or rotary mixer overnight at $4\,^{\circ}$C. If the protein is sufficiently stable, the reaction will proceed faster at room temperature. Some sites label faster and more completely than others and therefore some testing is generally required for each new labeling experiment. A surface-exposed site should label within minutes even at a 1:1 ratio; however, some buried sites require excess label and may take 16–24 h or more. Unreacted spin label is removed by extensive dialysis or repurification by affinity or desalting column chromatography. As discussed below, free spin label in solution has a very sharp signal and thus even small amounts of free label will be evident in the spectrum, so it is important to remove all the excess spin label before performing SDSL experiments.

As an essential first control, the cysteine-free protein should be expressed, purified, and subjected to the labeling reaction prior to adding new cysteines. This will allow one to determine if there are protein contaminants in the preparation that react with the label, and to assess the need for modifying the purification protocols to prevent background labeling problems. In addition, all reducing agents, such as dithiothreitol, need to be removed from the protein solution prior to labeling with spin label, since the reducing agents will cleave the newly formed disulfide bond formed between the spin label and the cysteine. In some cases, DTT can remain in the solution at concentrations significantly below that of the added spin label.

For electron paramagnetic resonance (EPR) experiments on spin-labeled proteins or peptides, the ideal concentration range for the spin label is 50–200 μM to give a good signal. Lower concentrations can also be used—down to 5–10 μM, for example—but require more acquisition time due to the need for more signal averaging, which is discussed below. The EPR machine detects only unpaired electrons, and in the majority of cases the spin label will be the only stable free radical present in the system. Therefore, in spin labeling experiments, at room temperature, the presence of nonparamagnetic contaminants such as lipids, detergents, buffer components, or other proteins do not add to the resulting EPR signal.

Sample volumes vary by technique and resonator or cavity choice. For experiments performed in a loop-gap resonator (LGR), the sample volumes used are typically about 2 μl, whereas in standard rectangular cavities the volumes used are typically 10–25 μl. Samples are contained in glass capillaries or custom plastic Polymethylpentene (TPX) sample holders and are fully recoverable after data acquisition. An example experiment in a cavity would be to record the spectrum of 15 μl of a singly spin-labeled 65-kDa protein at a concentration of 100 μM, which is less than 100 μg of protein. Or, for experiments in an LGR where only 2 μl is required, the experiment uses less than 15 μg of protein and each protein sample can be recovered. If sufficient sample is available or if the system under study cannot be concentrated, larger volumes can be accommodated in quartz flat cells (100–250 μl) or in sample configurations consisting of bundles of capillaries (0.25–1.0 ml), providing improved signal-to-noise ratios.

The main components of an EPR machine include a magnet to generate the magnetic field, a microwave source, a cavity or resonator to hold the sample, and a computer for data acquisition and analysis (Fig. 2). In traditional EPR

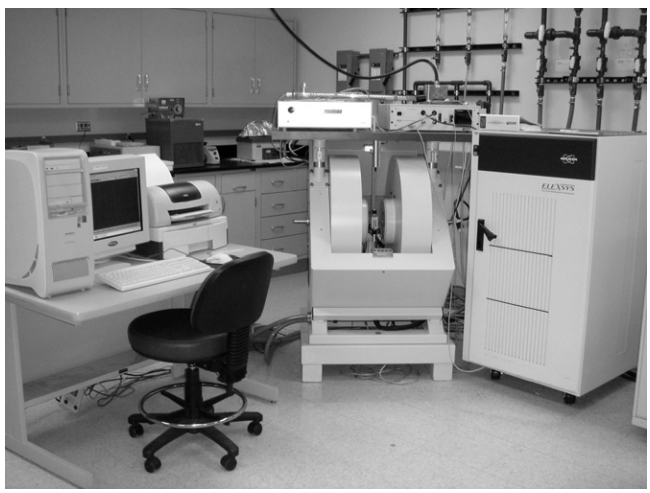

Fig. 2 A typical EPR machine setup with a magnet and microwave source (center), a power supply (right), and a computer for data acquisition (left).

experiments, the magnetic field is swept, typically over a range of 100 Gauss, and the microwave frequency remains constant. Gauss (G) is the unit of magnetic field that has been traditionally used in EPR spin labeling (1 G = 10^{-4} T). The vast majority of SDSL experiments are done at an operating frequency of ~9.5 GHz (referred to as X-band). Cavities are generally used for routine recording of spectra, while LGRs are used for experiments with limited amounts of sample and gas exchange experiments requiring saturating levels of microwave power.

EPR detects the absorption of microwave photons by the sample at specific resonant frequencies. In the presence of a magnetic field, an electron can exist in either of the two energy states (which may be thought of conceptually as aligned with or against the magnetic field) and, as shown in Fig. 3, the separation between the allowed energy levels (ΔE) for the electron spin increases as the magnetic field (H_o) is increased. When the energy difference between the two levels exactly matches the energy of the microwave radiation ($\Delta E = h\upsilon$), transitions between the spin states occur (as indicated by the vertical line in Fig. 3). If there are no interactions of the free electron with nearby nuclei, the EPR spectrum consists of a single line, as shown in Fig. 3.

For nitroxide spin labels, the unpaired electron interacts primarily with the nitrogen nucleus. This is referred to as the hyperfine interaction, and it produces small changes in the allowed energy levels of the electron that depend on the nuclear spin state, splitting the EPR signal into multiple lines. Spin labels with the predominant ^{14}N isotope give rise to a three-line EPR spectrum like the one shown in Fig. 4; the $I = 1$ nucleus splits the signal into $2I + 1$ lines (with each line corresponding to a different state of the ^{14}N nucleus). The nearby ^{16}O and ^{12}C nuclei have nuclear spins of zero and therefore do not contribute to additional line splitting (although under high-resolution conditions, splitting due to natural abundance ^{13}C, with $I = 1/2$, can be observed). Hyperfine interactions with the methyl group protons ($I = 1/2$) also occur but are typically too small to be resolved.

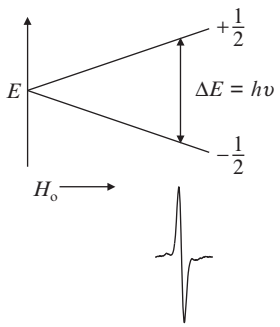

Fig. 3 EPR detects the absorption of microwave photons by the sample at a specific resonant frequency (υ). When the difference between the two energy levels (ΔE) exactly matches the energy of the microwave radiation ($h\upsilon$), transitions between the spin states occur, as shown by the vertical line, which corresponds to an EPR signal (shown below energy diagram).

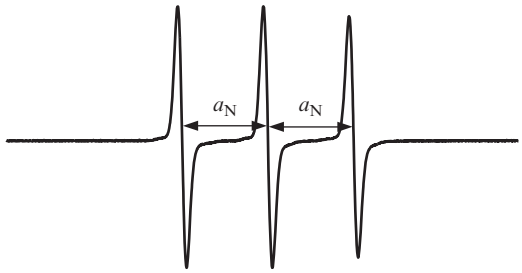

Fig. 4 Three-line nitroxide EPR spectrum. The ^{14}N isotropic hyperfine coupling constant a_N is given by the separation between the lines.

The remaining nuclei in a typical spin label are too far away (i.e., contain too little unpaired electron spin density) to significantly contribute to the spectrum.

The magnitude of the hyperfine interaction depends on the amount of unpaired electron spin density at the nucleus, and for spin labels varies as a function of the polarity of the microenvironment surrounding the nitroxide. Polar solvents, such as water, increase polarization of the N–O bond, resulting in increased electron spin density at the nitrogen nucleus and an increase in the nitrogen isotropic hyperfine coupling constant, a_N (Fig. 4). Spin labeling was one of the earliest techniques used to demonstrate the existence of a polarity gradient in membranes (Griffith and Jost, 1976; Hubbell and McConnell, 1968), and variation in a_N has been used as an indicator of bilayer depth for lipid-analogue labels (Marsh, 2001) and spin-labeled side chains in proteins (e.g., Zhang and Shin, 2006).

To improve the signal-to-noise ratio, a small (typically ~1 G) 100-kHz modulation of the magnetic field is applied and the detector filters out any signals that do not have this 100 kHz encoding. This results in a display of the EPR spectrum that is the first derivative of the original absorption spectrum (as indicated in Figs. 3 and 4). The corresponding absorption spectrum can be obtained if desired by simple integration of the first-derivative display.

There are three main categories of information that can be gained from SDSL EPR experiments: motional dynamics (due to the motion of the protein, the spin-label side chain, and/or the protein backbone), the accessibility of the spin label to paramagnetic broadening reagents, and distances between two introduced spin labels. Each of these categories of information is presented in detail below.

B. Motion

Among the most informative, and simplest, types of information that can be extracted from an EPR spectrum are parameters that reflect spin label motion. Since rotational mobility is encoded in the EPR lineshape, this information is obtained simply by acquiring the spectrum. Conventional, X-band EPR spectra are sensitive to rotational motion in the range of 0.1 to ~100 nsec. Specialized techniques such as saturation transfer (ST) EPR can extend the motional sensitivity to the millisecond timescale and are useful for determining the tumbling rate of

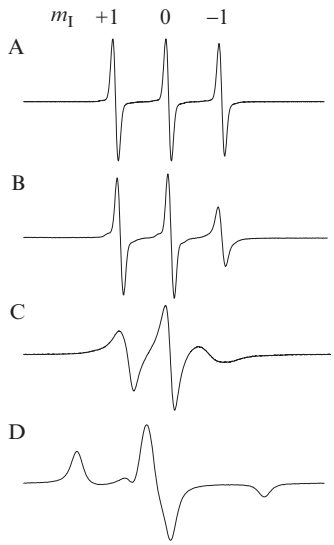

Fig. 5 The EPR spectrum is sensitive to the motion of the spin label side chain. (A) A dilute solution of MTSL, (B) MTSL bound to a small, 15-residue peptide in aqueous solution, (C) the same spin-labeled peptide folded into an α-helix, and (D) the spin-labeled peptide in frozen solution.

the spin-labeled protein as a whole or of a protein domain in a supramolecular complex (e.g., Fajer, 2000).

A series of EPR spectra corresponding to different rates of rotational motion are shown in Fig. 5. In the fast motional limit (~0.1 nsec), one observes three lines of approximately equal height (Fig. 5A). As the motion slows, the lines broaden (Fig. 5B and C). Since the intensity of each line is proportional to the product of its amplitude and the square of its width (i.e., $I \sim A\Delta H^2$), as the lines broaden their amplitudes decrease. As seen in Fig. 5, this broadening and decrease in amplitude varies for each of the three lines. The spectrum in Fig. 5D corresponds to the slow motion limit (>100 nsec) for conventional, first-derivative spin label EPR spectra. Referred to as a "powder" or "rigid limit" spectrum, this general shape is obtained for any nitroxide in the absence of rotational motion (and for a dilute powder or frozen solution).

As can be seen in Fig. 5B, attachment of the spin label to even a small, unstructured peptide results in some degree of motional restriction, and this restriction increases significantly in the presence of local secondary structure (Fig. 5C). Ultimately, the overall mobility of the spin label is determined by a combination of (1) motion of the label itself relative to the peptide backbone, (2) fluctuations of the α-carbon backbone, and (3) rotational motion of the entire protein or peptide. Using appropriate conditions, it is generally possible to isolate these various sources of spin label dynamics.

For proteins with molecular weights greater than ~15 kDa or proteins in macromolecular assemblies (including membrane proteins in cells, liposomes, or detergent

micelles), the overall tumbling rate of the complex is too slow to affect the conventional EPR spectrum. However, for proteins of less than ~15 kDa, rotational diffusion of the protein can influence the observed spectrum. That is, the spin label can be rigidly buried in the protein, and yet the spectrum may indicate fast-to-intermediate mobility due to tumbling of the entire protein or peptide. This can be simply overcome by adding solutes (e.g., sucrose or glycerol) that increase solution viscosity (e.g., Mchaourab *et al.*, 1997b). Addition of 30% sucrose increases bulk viscosity and dampens the Brownian rotation of the protein without significantly altering the motion of the nitroxide side chain.

Local fluctuations of the α-carbon backbone can also contribute to spin label mobility. This type of motion is evident from nuclear magnetic resonance (NMR) measurements on the relaxation of amide nitrogens (Palmer, 2001). To study backbone fluctuations by SDSL, the flexibility of the spin label side chain can be eliminated by using derivatives of MTSL with bulky substituents such as methyl or phenyl groups at the 4′ position of the nitroxide ring (Fig. 6) in place of hydrogen (Columbus *et al.*, 2001). Additionally, the effects of backbone fluctuations may be apparent when comparing sites in similar environments where side-chain flexibility is expected to be sequence-independent, as in the case of the α-helical zipper domain of the yeast transcription factor GCN4 (Columbus and Hubbell, 2002, 2004).

In most SDSL applications, it is the motion of the spin label side chain that is of primary interest, as it is this aspect of the motion that is sensitive to tertiary contacts and protein structure in the local environment of the spin label. There are five chemical bonds between the pyrroline ring of MTSL and the α-carbon backbone of the protein or peptide to which it is attached (see Fig. 6). A large number of studies with proteins of known structure, crystallographic analysis of spin-labeled proteins (Langen *et al.*, 2000), and spin labeling with MTSL analogues containing bulky substituents in the nitroxide ring (Columbus *et al.*, 2001) have indicated that at α-helical sites the flexibility of the side chain is dominated by rotations about the two bonds closest to the nitroxide ring moiety (X_4 and X_5). Interaction of S_δ of the disulfide bond with a backbone C_α hydrogen restricts mobility about the first two bonds adjacent to the α-carbon backbone, and isomerization about the disulfide

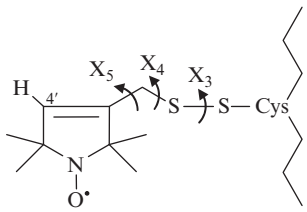

Fig. 6 A typical nitroxide side chain covalently bonded to a cysteine residue. The 4′ position of the nitroxide ring can be used to add bulky substituent groups to slow the rotation about the X_3, X_4, and X_5 bonds shown above.

bond (X_3) is slow on the EPR timescale, so that even at exposed helical sites the motion of the spin label is constrained to isomerizations about X_4 and X_5. In β-sheet proteins the situation is somewhat more complex, with spin label motion being influenced by location within the β-sheet (i.e., edge vs internal strand) and side-chain interactions with neighboring strands (Lietzow and Hubbell, 2004).

Crystal structures of T4 lysozyme (T4L) mutants labeled with MTSL indicated the presence of two favored conformations of the disulfide bond relative to the peptide backbone (Langen *et al.*, 2000). Because of these two alternative rotameric states of the MTSL side chain, EPR spectra may contain two motional components even though the protein is in a single conformational state (see Fig. 7). Nonetheless, the EPR spectral shape is still characteristic of the local structure, and changes in the relative amounts of the two motional components remain a sensitive indication of a change in protein conformation.

Although local secondary structure influences the spin label mobility somewhat, far more significant effects are seen at sites where the spin label is in tertiary contact with other side chains in the local environment. Spin labels at tertiary contact sites can exhibit complex spectral shapes (e.g., Fig. 7), and sites buried within the core of a large protein often approach the rigid limit.

As seen in Figs. 5 and 7, the effects of motion on the spin label spectrum are so dramatic that a given labeling site can often be classified as "mobile," "weakly immobilized," or "strongly immobilized" by casual inspection. However, motion can be quantitated quite precisely. For isotropic motion, the peak-to-peak width of each of the first-derivative lines, $\Delta H(m_I)$, is related to the rotational correlation time, τ_c (Stone *et al.*, 1965), such that

$$\Delta H(m_I) \propto [A + B(m_I) + C(m_I)^2]\tau_c + X \tag{1}$$

The constants *A, B*, and *C* are characteristic of the given spin label and are related to the anisotropy (orientation dependence) of the *g* and hyperfine values, while *X*

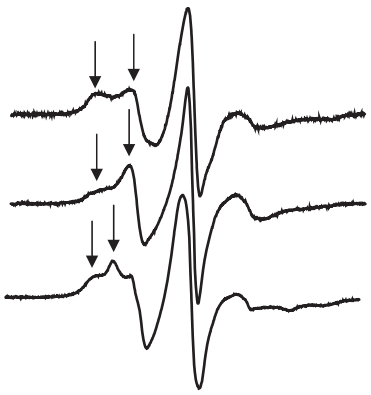

Fig. 7 Composite EPR spectra containing multiple motional components (indicated by arrows).

represents contributions to the linewidth that are not dependent on motion. The dependence of the linewidth on the nuclear spin state (m_I) indicates that each line will have a different width (e.g., Fig. 5C). The "A" term broadens all lines equally; the "C" term broadens the low- and high-field lines but does not affect the center line (for which $m_I = 0$); the "B" term is negative for spin labels and causes the high-field ($m_I = -1$) line to broaden and the low-field ($m_I = +1$) line to narrow. These various contributions give rise to the typical asymmetry seen for intermediate motion in Fig. 5. The rotational correlation time, τ_c, is the time necessary for the spin label to rotate through an angle of 1 radian, so that shorter times (smaller values of τ_c) indicate faster motion. The dependence on τ_c indicates that as motion decreases (i.e., τ_c increases) the lines broaden, and the greater the increase in τ_c, the more pronounced the linewidth asymmetry becomes (see Fig. 5).

In the intermediate-to-fast motional regime, where one observes three distinct first-derivative lines (e.g., Fig. 5A–C), an approximate value of τ_c is given by:

$$\tau_c = 6.5 \times 10^{-10} \Delta H_{pp}(0) \left[\left(\frac{A(0)}{A(-1)} \right)^{1/2} - 1 \right] \tag{2}$$

where $A(0)$ and $A(-1)$ are the peak-to-peak heights of the center- and high-field lines, respectively, $\Delta H_{pp}(0)$ is the peak-to-peak width of the center line, and τ_c is in seconds. The constant value is derived using the magnetic parameters of a small water-soluble nitroxide, *t*-butyl nitroxide. Although Eq. (2) is only an approximation, correlation times calculated from Eq. (2) do accurately reflect *relative* mobilities and *changes* in the spin label motion.

An even simpler parameter for examining relative mobility is the inverse width of the center line, $\Delta H_{pp}(0)^{-1}$. Since linewidth increases with decreasing motion (i.e., as correlation times become longer), taking the inverse width gives an empirical parameter that is proportional to motion. Since the center line is the narrowest (and hence has the greatest amplitude), the use of $\Delta H_{pp}(0)^{-1}$ allows one to evaluate motion from the most easily measured features of the spectrum (which can be beneficial in cases where signal intensity is limited). The inverse linewidth provides a measure of relative mobility so that when scanning through a region of secondary structure that is packed asymmetrically, one observes a periodicity in $\Delta H_{pp}(0)^{-1}$ that reflects the local structure. Similarly, if one is investigating a possible conformational change at a given site—for example upon ligand binding or protein folding/denaturation—an increase in $\Delta H_{pp}(0)^{-1}$ indicates increased mobility at that site and vice versa.

The inverse width of the center line can also be normalized to provide a scaled mobility parameter, M_S (Hubbell *et al.*, 2000), such that:

$$M_S = \left[\frac{\Delta H_{pp}(0)^{-1} - \Delta H_{pp}(0)^{-1}(i)}{\Delta H_{pp}(0)^{-1}(m) - \Delta H_{pp}(0)^{-1}(i)} \right] \tag{3}$$

where $\Delta H_{pp}(0)^{-1}(m)$ and $\Delta H_{pp}(0)^{-1}(i)$ are the inverse widths of the center line for the most mobile and most immobile sites in a given system, respectively. Thus, M_S is scaled to values between 0 and 1, with larger values indicating greater mobility. The scaled mobility can be useful for comparing local regions of secondary structure in disparate systems. For example, a plot of M_S for a series of sites in colicin E1 and annexin indicates that while both have α-helical secondary structure, the colicin E1 helix has greater mobility (Columbus and Hubbell, 2002).

A different set of parameters is used to characterize the spin label mobility in the slow motional regime. Such spectra are characterized by features corresponding to spin labels aligned with their z-axis parallel to the external magnetic field, separated by $2T_{\|}$, and those spin labels aligned with their xy plane along the direction of the magnetic field, separated by $2T_{\perp}$ (Fig. 8). Rotational motion causes the $2T_{\|}$ features to shift toward the center of the spectrum, so that the smaller values of $2T_{\|}$ indicate increased mobility and larger values of $2T_{\|}$ indicate that the motion of the nitroxide side chain has become even more restricted.

The sensitivity of the EPR spectrum to the spin label mobility is influenced by both the rate and the amplitude of the motion, and in general the rotational motion of a spin label is not isotropic (i.e., does not have the same amplitude in all directions). Indeed, even at exposed α-helical sites restriction of the internal side-chain dynamics to changes about the X_4 and X_5 bonds will limit the amplitude of the motion. Spin label motion is typically modeled as rotation within a cone about the z-axis (i.e., the nitrogen p-orbital; Fig. 9). The amplitude of the motion is described by an order parameter, S, such that,

$$S = \frac{1}{2}(3\langle \cos^2\ \theta\rangle - 1) \tag{4}$$

where $\langle \cos^2 \theta\rangle$ is the time-averaged value for the angle of deviation of the nitroxide z-axis. Note that for θ equal to 0°, $\langle \cos^2 \theta\rangle$ is 1 and the order parameter is 1, while for θ equal to 90°, $\langle \cos^2 \theta\rangle$ is 1/3 and the order parameter is 0 (i.e., the motion is isotropic). For experimental spectra with distinct $T_{\|}$ and $T_{\perp}$ features (such as Fig. 8), the order parameter can be determined from the relationship

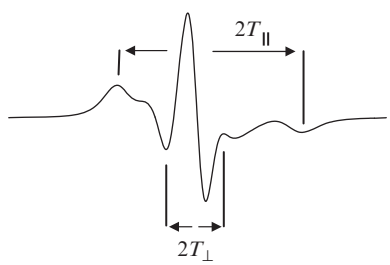

Fig. 8 A conventional, first-derivative EPR spectrum in the slow motional regime can be characterized by the motional parameters $2T_{\|}$ and $2T_{\perp}$, which can be used to calculate the order parameter.

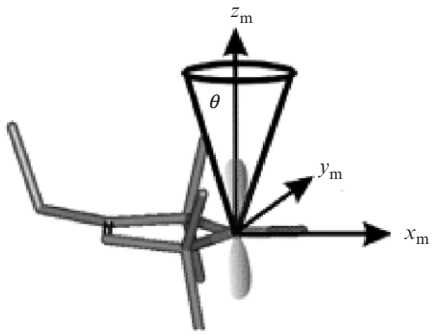

Fig. 9 The free electron in a nitroxide resides mainly in the nitrogen p-orbital, which is defined as the z-axis. Motion can be defined by the movement within a cone with a maximum angle θ about the z-axis.

$$S = \left[\frac{(T'_{||} - T'_{\perp})}{(T_{||} - T_{\perp})x_l}\right]\left[\frac{a_N(x_l)}{a'_N}\right] \tag{5}$$

where primes indicate experimental values and "x_l" indicates values determined from single-crystal or powder spectra. For spectra such as those in Fig. 8, the nitrogen isotropic hyperfine coupling constant, a_N, is given by $1/3(T'_{||} + 2T'_{\perp})$, and the factor $a_N(x_l)/a'_N$ is used to correct for differences in the experimental a_N relative to the $a_N(x_l)$ value observed in a single-crystal. More detailed discussions of the order parameter and its application to the anisotropic motion (i.e., preferential motion about a given direction, such as rotation about the long axis of a lipid alkyl chain) of lipid-analogue spin labels in membranes can be found in Gaffney (1976), Griffith and Jost (1976), and Hubbell and McConnell (1968).

For the majority of SDSL studies, measurements of relative mobility along a sequence (to establish secondary structure) or following some perturbation such as ligand binding (to follow changes in conformation) are sufficient to provide the structural information needed to understand a given biological mechanism. However, it is possible to obtain a more detailed description of the spin label side chain motion by simulating the EPR spectrum. For example, a simulation program based on microscopic order—macroscopic disorder (MOMD) has been developed (Budil *et al.*, 1996) that provides both rotational correlation times and order parameters for a given spectrum. The MOMD program has been used to examine the effects of the side chain structure on spin label motion in α-helices (Columbus *et al.*, 2001) and in an antiparallel β-sheet (Lietzow and Hubbell, 2004).

C. Accessibility

The power saturation technique takes advantage of the fact that certain reagents are paramagnetic and affect the relaxation rate of the spin label. Under nonsaturating conditions, the height of the spectral lines is proportional to the incident

microwave power, increasing linearly with the square root of the incident power, $P^{1/2}$. However, if high enough powers are used, the sample cannot relax fast enough to absorb additional photons and the increase in signal amplitude becomes less than linear with $P^{1/2}$, and at even higher microwave powers signal heights will begin to decrease. This phenomenon is referred to as saturation of the signal. When paramagnetic relaxation reagents interact with the spin label, they enhance the relaxation rate and allow the sample to absorb more power before becoming saturated. This process is a direct reflection of the bimolecular collision rate between the spin label and the paramagnetic relaxation agent, and provides valuable information about the environment of the introduced spin label. Conceptually, SDSL accessibility experiments are similar to fluorescence quenching, although the processes underlying the two techniques are fundamentally different.

Two main reagents are most commonly used: oxygen is small and hydrophobic and is generally found in the center of lipid bilayers and in hydrophobic pockets of proteins, and only to a small extent in the solution phase. Nickel compounds, such as nickel (II) ethylenediaminediacetate (NiEDDA), are water soluble and are located mainly in the solution phase and not found in the center of bilayers. NiEDDA is a neutral water-soluble compound and therefore does partition slightly into bilayers and hydrophobic regions, but another less commonly used paramagnetic broadening reagent is chromium oxalate (CROX), which is negatively charged and is strictly found in the aqueous phase. The natural relaxation rate of the spin label in a particular environment is measured in the presence of nitrogen, typically using N_2 flowing over a gas-permeable sample capillary to purge the sample of air. The degree to which the spin label interacts with each of these reagents can give us valuable information on its environment. The individual site can be located within a bilayer, buried within a protein, or on a solvent-exposed surface based on this type of data.

The accessibilities of a particular spin label to oxygen and NiEDDA can be determined by power saturation methodology where the height of the center line of the spectrum is measured at a series of microwave powers. First, the sample is inserted into a small gas-permeable plastic (TPX) sample tube, and after insertion into the LGR, nitrogen or oxygen gas is continuously blown over the sample to equilibrate the sample with either nitrogen or 20% oxygen. For the control and for samples containing the NiEDDA reagent, the sample is equilibrated with nitrogen, whereas air is used for the introduction of oxygen into the sample. For each sample, the height of the center line is recorded in the presence of nitrogen as a control, in the presence of 20% oxygen (air), and with the addition of 5- to 200-mM NiEDDA to the protein solution and recorded under nitrogen gas. This requires only one or two samples since the nitrogen and air experiments can be done on the same sample simply by changing the gas flowing over the sample, and the NiEDDA experiment can be carried out using a new sample or by addition of reagent to the recovered nitrogen/air sample.

Once the gas is equilibrated, the range of powers typically required is 0.5–100 mW, but this strongly depends on the configuration of the spectrometer,

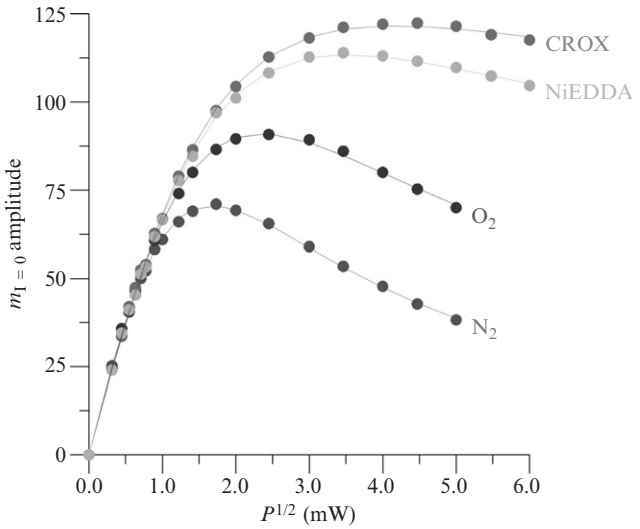

Fig. 10 Typical CW saturation plots for a sample in the presence of various paramagnetic broadening reagents. This particular spin label is in a water-soluble environment, based on the fact that it takes longer for the EPR signal amplitude to become less than linear with power in the presence of the water-soluble reagents CROX and NiEDDA than in the presence of hydrophobic oxygen. A power saturation curve is always run in the presence of nitrogen as a baseline value. These curves can be fitted to Eq. (6) to obtain a quantitative power saturation value, $P_{1/2}$.

the resonator properties, and the degree of accessibility of the site being studied. The central lineheight is then plotted against the square root of the incident microwave power (Fig. 10) and fitted to the following equation, which yields a $P_{1/2}$ value (Yu *et al.*, 1994).

$$A = IP^{1/2}\left[\frac{1 + (2^{1/\varepsilon} - 1)P}{P_{1/2}}\right]^{-\varepsilon} \tag{6}$$

$P_{1/2}$ is the power at which the intensity of the first-derivative center lineheight is half of its unsaturated intensity and is referred to as the power saturation parameter. A is the height of the center line, I is a scaling factor, P is the incident microwave power, and ϵ is a line homogeneity factor. The resulting $P_{1/2}$ value for the nitrogen control is subtracted from both $P_{1/2}(O_2)$ and $P_{1/2}$(NiEDDA) to generate $\Delta P_{1/2}$ values that quantitate the degree of accessibility to oxygen and NiEDDA, respectively (Altenbach *et al.*, 1989). That is, for NiEDDA

$$\Delta P_{1/2}(\text{NiEDDA}) = P_{1/2}(\text{NiEDDA}) - P_{1/2}(N_2) \tag{7}$$

The $\Delta P_{1/2}$ value is a direct measure of the bimolecular collision rate between the spin label side chain and the paramagnetic relaxation agent, which yields accessibility information at a very local site. $\Delta P_{1/2}$ values can be normalized to account for spectrometer configuration, resonator properties, and spectral linewidth to give the accessibility parameter, Π, using diphenylpicrylhydrazyl (DPPH) as a standard for calibration (reviewed in Feix and Klug, 1998; Klug and Feix, 2004). Π is a dimensionless parameter that essentially translates the $\Delta P_{1/2}$ values into universal values that can be compared across different labs and proteins.

Standard cavities are not normally suitable for power saturation studies because they do not provide high enough powers to adequately saturate the sample. LGRs concentrate the microwaves within the resonator, allowing one to attain saturating conditions. The incident microwave power (P) and the microwave field generated within the resonator or cavity (H_1) are directly related by a $\wedge$ factor: $H_1 = \wedge P^{1/2}$. Cavities tend to have a $\wedge$ value of $\sim$1, while for LGRs, $\wedge$ is $\sim$5–8, significantly increasing the microwave field experienced by the sample.

As an example of this technique, a solvent-exposed site on a protein would give a very high $\Delta P_{1/2}$ value in the presence of NiEDDA, whereas a site exposed to the lipid phase near the center of the bilayer would yield very high oxygen $\Delta P_{1/2}$ values, but very small $\Delta P_{1/2}$ values for NiEDDA. For example, from the data in Fig. 10, one can immediately identify the site as being solvent exposed because it is visibly apparent that it takes longer to saturate the EPR signal in the presence of the water-soluble reagents NiEDDA and CROX than it does in the presence of hydrophobic oxygen. In addition to important information on the environment of specific sites within a protein or peptide, a series of consecutive sites can be individually studied to produce secondary structure information. This method, where the accessibility values are plotted against position number, can distinguish between α-helical, β-strand, and unstructured regions of a protein. This works because external α-helices have a periodicity of 3.6 residues per turn, so every 3 or 4 residues would be highly exposed to the solvent (showing high NiEDDA values), and the sites on the other side of the helix would be buried against the protein and show low $\Delta P_{1/2}$ values for both NiEDDA and oxygen (see Fig. 11). Similarly, β-strands give a periodicity pattern of 2.0 (Fig. 11), and unstructured regions will show no regular periodicity. Sequences buried within a protein or elements of secondary structure that lack any tertiary contacts would not be differentiated using this technique as all sides of the structure would be either completely inaccessible or fully accessible to the reagents used, respectively. In-phase periodicities of oxygen and NiEDDA data indicate solvent-exposed structural elements, whereas out-of-phase periodicities of the oxygen and nickel accessibilities identify lipid-exposed structural elements.

For integral membrane proteins or membrane-associated peptides, the depth of a given spin label side chain within a lipid bilayer can be determined using accessibility data based on the inverse concentration gradients of oxygen and NiEDDA within a lipid bilayer. This is an extremely useful technique for positioning protein or peptide segments within the lipid bilayer (e.g., Hubbell *et al.*, 1998;

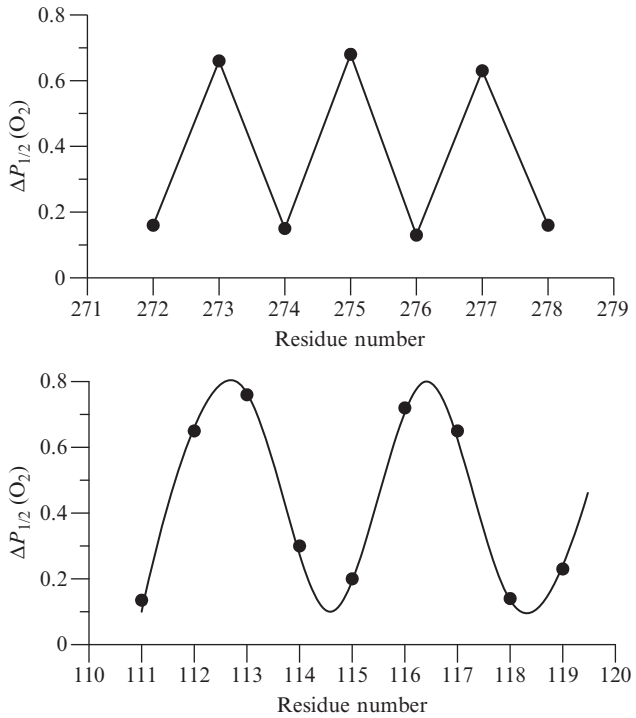

Fig. 11 Idealized accessibility data plots indicating β-strand and α-helical secondary structure.

Isas *et al*., 2002; Perozo *et al*., 2001; Zhao *et al*., 1999). In order to obtain depth measurements of spin label side chains facing the membrane, another parameter, Φ, is calculated based on the following equation (Altenbach *et al*., 1994):

$$\Phi = \ln\left[\frac{\Delta P_{1/2}(O_2)}{\Delta P_{1/2}(\text{NiEDDA})}\right] \tag{8}$$

The variation in the concentrations of oxygen and NiEDDA within the membrane bilayer has been shown to be inversely proportional (Altenbach *et al*., 1994); oxygen concentration is greatest at the center of the bilayer and decreases toward the membrane surface, whereas NiEDDA concentration is greatest at the surface of the bilayer in the aqueous phase and decreases to nearly zero in the center of the bilayer. Therefore, the natural log of this ratio yields Φ, a parameter with a linear dependence on depth into the bilayer. Φ can then be calibrated to each particular membrane system using lipid-analogue spin labels that localize at known bilayer depths (e.g., Fig. 12). Membranes containing unlabeled wild-type proteins are calibrated with the addition of 0.5–1 mol% spin-labeled lipids (relative to host lipid). 5-, 7-, 10-, and 12-doxyl PC lipids (Avanti Polar Lipids) contain

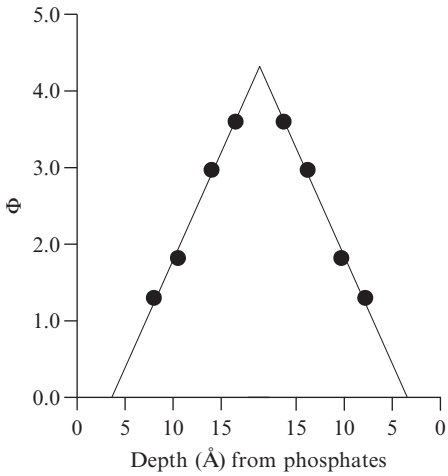

Fig. 12 Example of a bilayer depth calibration using 5-, 7-, 10-, and 12-doxylPC spin labels. This system, which contained reconstituted, unlabeled FepA, yielded a calibration equation of $Å = 3.56\Phi + 3.62$ (Klug *et al.*, 1997).

a spin label at the indicated positions and have known depths in the bilayer (Dalton *et al.*, 1987). The accessibility measurements obtained for each lipid label and their Φ values are plotted against their known depths to yield a bilayer depth calibration equation:

$$\text{depth}(Å) = m\Phi + b \tag{9}$$

The resulting equation is used to calculate the depth of membrane-exposed residues of integral membrane proteins and peptides, based on their respective Φ values (as in Fig. 12; Klug *et al.*, 1997). Note that Φ values do not provide depths for sites not exposed to the lipid phase (e.g., buried within a helical bundle or facing an aqueous transmembrane channel). The resolution of this technique is limited only by the rotational range of the spin label side chain and is more than sufficient for insertion depths of specific sites within a protein or peptide in a membrane bilayer.

D. Distances

One of the most active, rapidly developing aspects of SDSL is the ability to make distance measurements between two spin labels, either intramolecular distances between two labels in the same monomer or intermolecular distances between sites on different proteins (for detailed reviews, see Borbat and Freed, 2000; Eaton *et al.*, 2000; Hustedt and Beth, 2000; Xiao and Shin, 2000). Distance measurements between two nitroxides can provide information on both protein structure and

functional dynamics. Various methodologies have been developed to study this interaction in biological systems in frozen solutions or at room temperature. The ability to monitor conformational changes within a large protein structure based on changes in spin–spin interactions (and, therefore, in the distances between the two labeled sites) is a unique benefit of this technique. Because SDSL distance measurements can be used to determine how regions of secondary structure are organized, it, in principle, allows the development of a full structural model based on EPR data alone. For SDSL distance measurements, both sites are typically labeled with a single type of label such as MTSL, as there is no requirement for distinct donor and acceptor probes (see Chapter 8 by Shanker and Bane, this volume for a parallel discussion of donor acceptor pairs in fluorescence measurements).

Distance measurements are based on observing the effects of magnetic dipolar interactions between the unpaired electrons of two spin labels (or of a spin label and a paramagnetic metal ion). This is a through-space interaction that is not influenced by intervening protein structure (an advantage relative to chemical cross-linking methods). In the range of ~8–20 Å, interactions between the magnetic dipoles of the two labels give rise to distance-dependent line broadening in the conventional continuous wave (CW) EPR spectrum. Line broadening is accompanied by a decrease in signal amplitude, and for distances up to ~15–20 Å a decrease in peak height for spectra normalized to the same spin concentration can often be used as a qualitative indication of spin–spin interaction (e.g., Fig. 13). In many cases, this is all that is necessary to determine oligomerization state or demonstrate a conformational change. For higher resolution structural analysis, quantitative distances can be determined using spectral simulation approaches based on Fourier deconvolution (Altenbach *et al.*, 2001c; Rabenstein and Shin, 1995), convolution of the spectra from noninteracting spins with a broadening function (Mchaourab *et al.*, 1997b; Steinhoff *et al.*, 1997), or by rigorously simulating spectra with consideration of both the distance between spin labels and their relative orientations (Hustedt *et al.*, 1997, 2006). The resolution limit of these

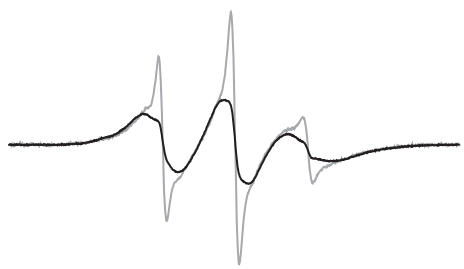

Fig. 13 Spin–spin broadening. The gray line represents the sum of the two single mutant spectra, and the black line represents the broadened spectrum resulting from dipolar interaction between the two spin labels in the double mutant.

methods is determined primarily by the distribution of distances between spin labels that arises because of the inherent flexibility of the nitroxide side chain and is typically on the order of 1–2 Å. For highly immobilized, well-oriented pairs of spin labels, a resolution of 0.1–0.2 Å has been achieved (Hustedt *et al.*, 1997).

Recently developed pulse EPR methods, including pulse electron–electron double resonance (DEER or pELDOR) (Brown *et al.*, 2002; Pannier *et al.*, 2000; Steinhoff *et al.*, 1997; Zhou *et al.*, 2005) and double quantum coherence (DQC) (Bonora *et al.*, 2004; Borbat and Freed, 2000; Borbat *et al.*, 2001, 2002) have now made possible the measurement of interspin distances in the range of ~20–60 Å. This increase in range has greatly expanded potential applications. With this increased sensitivity, the researcher has significantly more flexibility in deciding where to place the spin labels and can now choose nonperturbing sites, such as on the outer surface of an exposed helix. In this approach, a second microwave frequency is used to perturb the relaxation of a saturated spin label, resulting in modulation of its time-dependent signal intensity (Fig. 14). Analysis of the depth and frequency of modulations provides a distance between the two labels. In addition, the width of the derived distance distribution contains information on structural heterogeneity, that is, a narrow distance distribution indicates that the protein is structurally homogeneous and that the spin labels occupy a narrow range of orientations with respect to the peptide backbone. At present, the need for

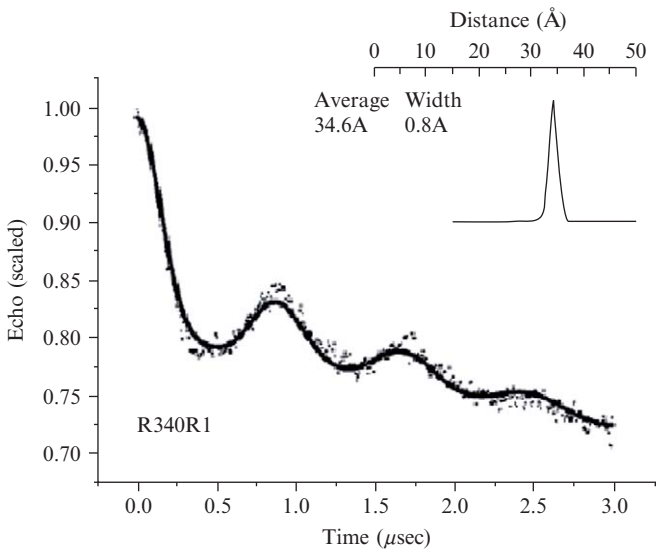

Fig. 14 Example of a DEER spin echo distance distribution measurement. Reprinted with permission from Zhou *et al.* (2005). Copyright 2005 American Chemical Society.

sufficiently long relaxation times requires these measurements to be made at liquid N_2 temperature (77 K) or lower; a number of studies have indicated that rapid freezing in the presence of a suitable cryoprotectant (e.g., glycerol or sucrose) generally preserves the relevant structure.

II. Examples

In this section, we illustrate the practical applications of the SDSL methods described above through specific examples in the literature. Although only a very small set of the many published experiments using SDSL are used here as illustrations of the usefulness of the technique, a variety of reviews also exist to readily point out additional experiments (e.g., Borbat *et al.*, 2001; Feix and Klug, 1998; Freed, 2000; Hubbell *et al.*, 1998, 2000; Hustedt and Beth, 1999; Klug and Feix, 2004; Millhauser, 1992; Thompson *et al.*, 2001).

A. Secondary Structure

The secondary structural elements of a section of protein can be determined by nitroxide scanning through the region of interest and plotting the accessibilities or motional parameters of each spin-labeled site as a function of sequence position. Useful information includes not only the secondary structure of the sites studied, but can also indicate changes in structure or lack of structure. Examples of each type of secondary structural element as determined mainly by power saturation EPR are presented below.

1. α-Helix

One of the most studied proteins by SDSL is T4L, which is a highly helical protein as determined by X-ray crystallography. It is known as the workhorse for the SDSL technique and was first used as a model helical protein to demonstrate the effectiveness of the accessibility approach to structure determination by EPR (Hubbell *et al.*, 1996). A set of eight consecutive residues on an external helix were individually spin labeled and their accessibilities to the paramagnetic broadening reagent oxygen were plotted versus sequence number. The data points could be overlaid with a sine wave with a periodicity of 3.6, clearly demonstrating the capability of the technique to correctly identify α-helical secondary structure. This study also indicated that the introduction of a spin label side chain does not significantly perturb the protein structure. It was also shown in this study that plotting the inverse of the central linewidth of the spectrum showed a similar periodicity, and this mobility parameter can often be used as an indicator of structure.

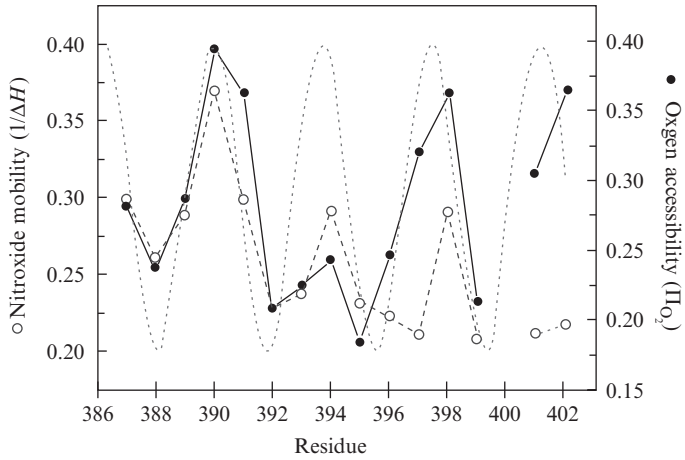

Fig. 15 Accessibility and mobility data are consistent with α-helical secondary structure, as indicated by the 3.6 residue periodicity (dotted line), for a stretch of residues in lactose permease. Reprinted with permission from Voss *et al.* (1996). Copyright 1996 American Chemical Society.

Another early example of the use of accessibility and mobility measurements to identify α-helical secondary structure is the study of lactose permease (Voss *et al.*, 1996). Fourteen sites in one of the 12 putative α-helices of lactose permease were spin labeled and analyzed by accessibility to oxygen and nitroxide mobility ($\Delta H_{pp}(0)^{-1}$). The data showed a periodic dependence of 3.6 for both the accessibility and the mobility parameters, directly supporting the idea that these residues form an α-helix (Fig. 15) and that it is located on the outside of the proposed helical bundle.

2. β-Strand

Cellular retinol-binding protein (CRBP) is a small water-soluble β-sheet protein with a known crystal structure that was first used to demonstrate the effectiveness of the SDSL power saturation technique in identifying β-strand secondary structure (Hubbell *et al.*, 1996; Lietzow and Hubbell, 1998, 2004). The accessibilities to oxygen for five consecutive sites on an external strand were plotted against residue number and the data clearly revealed a periodicity of 2.0. The sites with higher accessibility values corresponded to the solvent-exposed surface, while the sites with lower accessibilities were buried within the protein, allowing assignment of not only the secondary structure for this section of protein but also the fold.

The first studies on an integral membrane protein with a high content of β-strand secondary structure involved the ferric enterobactin receptor, FepA (Klug *et al.*, 1997). A nitroxide scan through a predicted transmembrane segment clearly

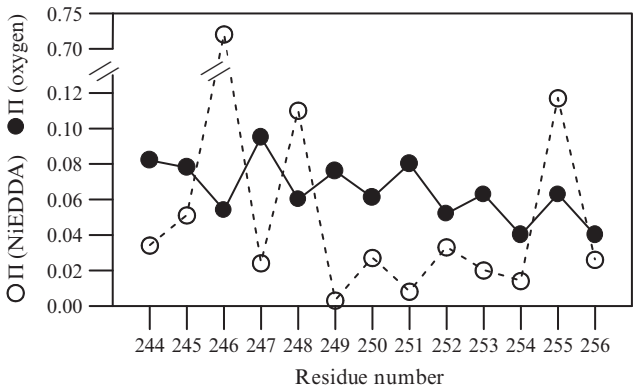

Fig. 16 Variation in the accessibility parameter Π as a function of spin label position in FepA. The alternating out-of-phase periodicity indicates residues 245–253 form a transmembrane β-strand. Note that the variation in accessibility becomes in-phase once the strand exits the bilayer (i.e., before 246 and after 253). Reprinted with permission from Klug and Feix (1998). Copyright 1998 Cold Spring Harbor Press.

demonstrated that sites 245–253 showed an alternating (2.0) periodicity in their accessibilities to oxygen and NiEDDA, proving β-strand structure, and also that the accessibilities were out-of-phase, indicating that the strand was located in a membrane environment (Fig. 16). Depth measurements (discussed below) confirmed that this β-strand spanned the bilayer. Identification of membrane interfaces is a particularly useful feature of SDSL. As seen in Fig. 16, accessibility to NiEDDA increases sharply at residues 246 and 255, indicating a transition from the membrane to the aqueous phase. FepA from *Escherichia coli* was subsequently crystallized (Buchanan *et al.*, 1999) and shown to be a transmembrane β-barrel protein with a large N-terminal plug domain filling the interior channel, and the location of the β-strand characterized by SDSL was confirmed in precise detail. This SDSL study also indicated unusually low NiEDDA accessibility, as well as low mobility, for residues facing the inside of the barrel (250–254). This was later accounted for by the presence of the 153-residue plug discovered in the crystal structure.

One of the highly conserved sequences within the soluble lens protein αA-crystallin was investigated as the first-soluble β-strand to be studied on an uncrystallized protein structure (Mchaourab *et al.*, 1997a). Analysis of 12 consecutive sites demonstrated that this conserved section of protein formed a β-strand based on a clear 2.0 periodicity in the accessibility data. One side of the strand showed very low accessibility to both oxygen and NiEDDA along with very slow motion, indicating that this face of the strand has extensive tertiary interactions within the protein. Although residues on the opposing face had higher accessibilities, they remained low relative to other systems. The authors concluded that this identifies sites of contact within the quaternary or oligomeric assembly of the protein subunits, giving additional insight into the folding of the protein beyond that of secondary structure information.

3. Changes in Structure

As well as identifying regions of secondary structure within a protein or peptide, the SDSL technique can also identify unstructured regions, which are characterized by a lack of regular periodicity in their accessibility plots. Also, changes in local structure can be monitored using this technique.

For example, a series of spin labels were introduced into the 140-amino acid protein α-synuclein, and their EPR spectra were recorded in solution and in the presence of membranes (Jao *et al.*, 2004). α-Synuclein is considered a natively unfolded protein, and previous analysis by circular dichroism suggested that the protein undergoes a conformational change from unstructured in solution to α-helical in the membrane-bound form. To investigate this structural change, numerous single cysteine mutants were constructed and spin labeled with MTSL. In solution, their EPR spectra showed very fast motion, clearly indicating that the protein is largely unfolded in this state. However, upon addition of membranes, the majority of the spectra became more immobile, confirming that a conformational change does occur. To characterize the secondary structure of this membrane-bound form, the authors determined the accessibilities to oxygen and NiEDDA for 32 consecutive residues. The data correspond to a regular α-helical structure with a periodicity of 3.67 amino acids per turn, remarkably similar to the ideal value of 3.6. In addition, a helical wheel representation of the residues studied was generated based on this periodicity, which revealed that this helix does indeed have a polar face that is solvent-exposed and a hydrophobic face that interacts with the membrane. The average immersion depth of the membrane-exposed helix side chains was determined from the saturation parameters to be ~11 Å for the entire helix, suggesting that it lays flat across the surface of the membrane.

Mobility can also be a useful tool for determining secondary structure and tracking changes in conformation. For example, sites in the N-terminal TonB box region of the vitamin B_{12} transporter BtuB were recorded in the absence and presence of ligand to identify the structural change that occurs in this region upon ligand binding (Hubbell *et al.*, 2000; Merianos *et al.*, 2000). When the mobility parameters (the inverse linewidths of the central line) for each spectrum are plotted in the absence of ligand, they show a periodicity that is consistent with α-helical secondary structure (Fig. 17). However, upon addition of ligand, mobility parameters at all sites become relatively similar and increase, suggesting loss of secondary structure and increased flexibility in the Ton box. These changes can be interpreted in terms of a proposed transmembrane signaling mechanism for BtuB (Merianos *et al.*, 2000).

B. Membrane Depth

The first example of measuring depths of spin labels within a membrane was published in 1994 and describes the methodology as applied to the transmembrane helical protein bacteriorhodopsin (Altenbach *et al.*, 1994). The authors make use

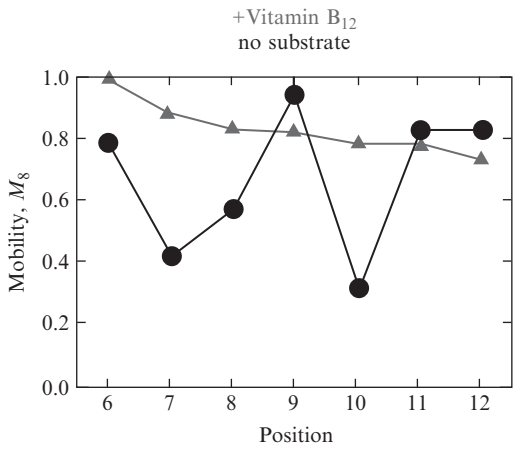

Fig. 17 Differences in mobility for residues in the TonB box of BtuB in the absence (circles) and presence (triangles) of ligand. Reprinted by permission from Macmillan Publishers Ltd, Hubbell *et al.* (2000).

of the fact that, for spin label side chains exposed to the lipid phase, the ratio of collision rates of the spin label with oxygen to that of a polar metal ion complex (e.g., NiEDDA) is independent of the structure of the protein, and that the logarithm of this ratio is linearly dependent on depth into a membrane bilayer. This ratio was measured for 10 sites on one of the membrane-exposed helices of bacteriorhodopsin and membrane depths relative to the lipid phosphate groups for each site were calculated. The depth parameter described earlier (Φ) was plotted versus residue number, and for the sites studied, increased up to position 117 and then began to decrease, indicating that site 117 is positioned in the center of the bilayer and the whole sequence spans the membrane. In addition, the distance between two of the outer helical sites (105 and 129) was experimentally determined by depth measurements to be 37 Å, which corresponds to the model distance of 37.5 Å (1.5 Å for each of the 25 residues) for an α-helix, revealing an additional layer of information in the depth data. This work nicely describes the theory behind this approach, which is now used routinely in the field as a relatively straightforward and unique method of measuring the depth of specific sites on a large protein within a lipid bilayer.

Another example of the practical application of this technique to membrane depth determinations is FepA, introduced above. In addition to confirming the biphasic periodicity of a section of putative transmembrane β-structure, depth measurements were determined for the membrane-exposed sites (Klug *et al.*, 1997). The depth parameter, Φ, was plotted for each site and clearly indicated that this region spans the membrane and that site 249 was located at the center of the bilayer, as shown in Fig. 18. Membranes containing spin-labeled lipids and unlabeled protein were used to derive a calibration equation as discussed in Section I.

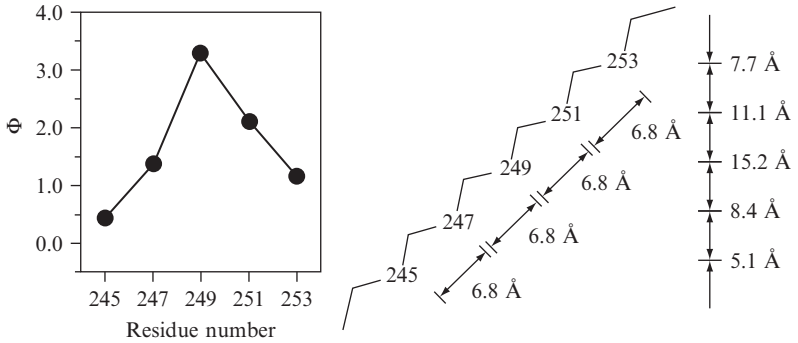

Fig. 18 (Left) A plot of the depth parameter versus residue number indicates that this sequence in FepA forms a transmembrane β-strand. (Right) Comparison of measured depths to β-strand secondary structure allows determination of strand tilt. Reprinted with permission from Klug *et al.* (1997). Copyright 1997 American Chemical Society.

Further, when depth measurements for the membrane-exposed sites were compared, the vertical distances between alternating strand sites were shorter than the model antiparallel β-strand distance of 6.8 Å, indicating that the strand was tilted relative to the bilayer normal (Fig. 18). Using the relationship $\cos \alpha = a/b$, where α is the strand tilt, a is the average experimentally determined vertical distance between residues, and b is the distance between residues in a β-strand, yielded a tilt angle of the strand with respect to the bilayer that was used to calculate a suggested diameter of 22 Å for this barrel, again in good agreement with that subsequently determined from the crystal structure (Buchanan *et al.*, 1999). Therefore, as illustrated in both of these examples, not only can individual depths be determined using SDSL but additional structural characteristics can be ascertained as well.

C. Protein Interactions

Spin label mobility is an excellent indicator of local protein folding characteristics and gives insights into protein dynamics and tertiary interactions (Farrens *et al.*, 1996; Hubbell *et al.*, 1996, 2000; Karim *et al.*, 1998; Klug and Feix, 1998; Klug *et al.*, 1995, 1998). Structural information in a protein can easily be followed using the SDSL method as the spectra of loop sites, helix surface sites, buried sites, and sites involved in tertiary contacts each have unique characteristics. Therefore, residues involved in protein–protein, protein–peptide, or protein–ligand contact sites can be readily identified by following changes in motion and/or spin–spin interactions of the spin label side chain(s). Examples are described below for systems previously studied by the SDSL technique and show that it is especially useful in the absence of crystal structures of biologically important protein complexes or for those that undergo dynamic changes in conformation not observable by crystal analysis.

1. Protein–Protein Interactions

Interactions between two different proteins can be studied by SDSL at the level of individual amino acids. As one example of the many studies between proteins, the visual protein arrestin was spin labeled at a variety of sites along its surface (Hanson *et al.*, 2006). The spectra were recorded for the protein alone in solution and then also in the presence of the light receptor, rhodopsin. Spectra were recorded in the presence of rhodopsin in the dark and then following light activation to identify which sites on arrestin were involved in binding each state of the receptor. The face of arrestin involved in the interaction between the two proteins was mapped out based on the changes in spin label mobility observed directly from the spectra. Even more specifically, individual sites in the C-tail of arrestin were identified as becoming more mobile upon binding to rhodopsin, indicative of a release of this region during binding, and sites found in a "finger" region that is proposed to insert into a cavity that opens in the receptor upon light activation became significantly more immobilized. In summary, the individual sites within arrestin that are affected by binding to its receptor were identified by changes in motion, and additional information on the conformational changes occurring in specific regions were also revealed, giving valuable characterization of this biological interaction.

The ability to observe spin–spin interactions in SDSL has also been exploited in studies of protein oligomerization. For proteins that form dimers or higher order oligomers, judicious placement of the spin label can be used to characterize the interface between monomers, and titration of spin-labeled protein with unlabeled protein can be used to determine the oligomerization state. An example of this type of SDSL application is the study of the assembly of annexins at the membrane surface (Langen *et al.*, 1998). Annexins exhibit reversible binding to phosphatidylserine-containing membranes in the presence of Ca^{2+}. Crystal structures of the soluble form indicated a variety of potential quaternary states, including monomers, dimers, trimers, and hexamers. To investigate the membrane-bound state, a number of sites were selected for spin labeling that were hypothesized to be close to a protein–protein interface based on existing crystal structures. In solution, the EPR spectra at these sites were characteristic of fast rotational motion. However, upon binding to membranes in the presence of Ca^{2+} spin–spin broadening was so extreme that the EPR signal for the membrane-bound state essentially disappeared into the baseline. To separate broadening due to spin–spin interactions from that due to changes in motion, spectra were also obtained for the membrane-bound state in the presence of a ninefold excess of unlabeled annexin. Dilution of the spin-labeled species significantly increased spectral amplitude, confirming that line broadening in the undiluted samples was due to spin–spin interactions within the oligomer. To further examine the oligomeric state of membrane-bound annexin, one of the spin-labeled mutants was carefully titrated with unlabeled protein. Changes in the amplitude of the center line as a function of the mole fraction of spin-labeled protein were compared to models based on binomial distributions for dimers, trimers, and hexamers. The

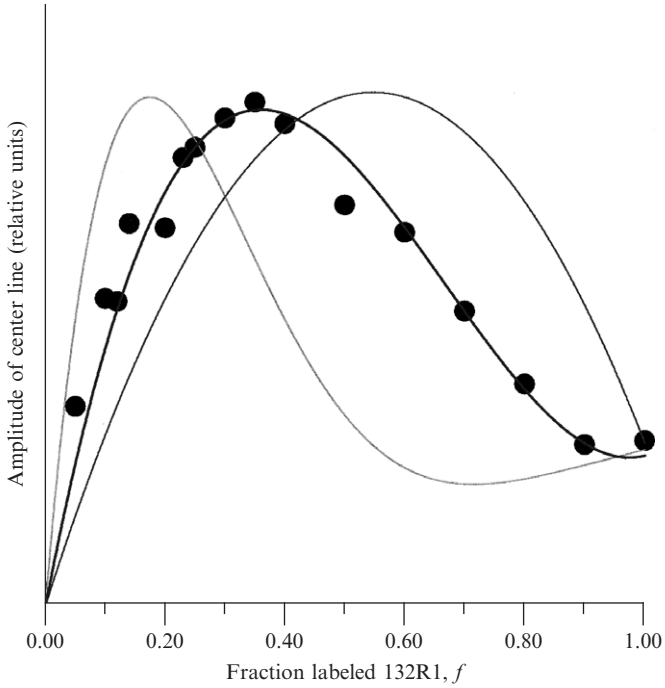

Fig. 19 Variation in EPR signal height with the fraction of spin-labeled protein for annexin 12 aligns with the binomial distribution expected for trimers, rather than dimers or hexamers. Reprinted with permission from Langen *et al.* (1998). Copyright 1998 ASBMB.

experimental data closely fit the distribution expected for trimers (Fig. 19), establishing the membrane-bound oligomeric state of annexin 12.

2. Protein–Ligand interactions

Similarly, interactions between a protein and its ligand can also be monitored by SDSL at very localized sites. Typically, the protein is spin labeled at specific sites proposed to interact with the ligand; however, the ligand can also be spin labeled and used as a probe itself (e.g., Beth *et al.*, 1984; Hustedt *et al.*, 1997). Few examples exist in the literature for spin-labeled ligands, though they are becoming more commonly synthesized and used in EPR binding studies.

As an example of a single site within a protein being studied to observe the effect of ligand binding, FepA was spin labeled at position 338, thought to be close to the ferric enterobactin-binding site and shown to be solution-exposed and within 4.5 Å of the lipid headgroups using accessibility data (Klug *et al.*, 1998). The ligand-induced change in the spin label motion at this site was significant, with the ligand-bound spectrum showing a marked decrease in motion to a spectrum

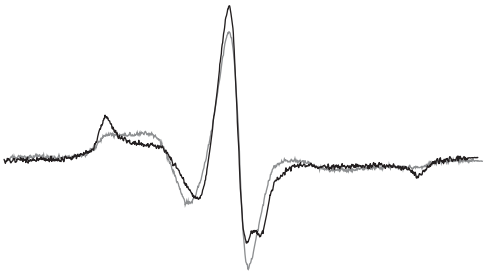

Fig. 20 Overlays of the FepA V338C spectra showing differences in mobility in the absence (gray) and presence (black) of ligand. Reprinted with permission from Klug *et al.* (1998). Copyright 1998 American Chemical Society.

indicative of extremely slow motion on the EPR timescale (Fig. 20). In addition, the accessibility data were used to show that this site becomes less accessible to the broadening reagents after ligand binding, further verifying that this site either is in direct contact with the ligand or is experiencing additional tertiary contacts due to structural rearrangement of the protein upon ligand binding.

As another example, the lipid A transporter, MsbA, was spin labeled at 13 consecutive sites within a known ligand-binding region of the protein to determine the role of each site in ligand binding (Buchaklian and Klug, 2005). The Walker A region of MsbA is a conserved sequence found in ATPases that is known to be involved in ATP binding and hydrolysis. Thus, it was not surprising that a number of the residues showed significant motional changes during the hydrolysis cycle. However, the exact sites affected by binding were clearly identified and indicated that the entire Walker A region is not affected by ATP binding. The results were not able to distinguish between direct contact with the ligand or structural rearrangements in this region; however, the added accessibility studies did verify that these sites were much less accessible to the broadening reagents upon ATP hydrolysis than they were in the resting state of the protein.

D. Peptides

1. Peptide–Membrane Partition Coefficients

SDSL has proven to be an extremely useful approach for the study of peptides that partition between the membrane and the aqueous phases. On membrane binding, a spin-labeled peptide typically undergoes a significant reduction in rotational mobility. Under conditions where there is an equilibrium distribution of peptides between the membrane and aqueous phases, one observes a superposition of signals from the two populations. This allows a simple and straightforward determination of the partition coefficient without having to separate bound and free peptide. Shown in Fig. 21 are EPR spectra of a 15-residue spin-

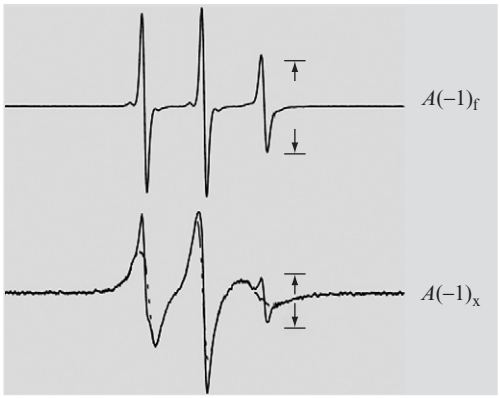

Fig. 21 EPR spectra of spin-labeled CM15 (above) in aqueous solution and (below) in equilibrium with liposomes. The dashed line in the bottom spectra is for peptide 100% membrane bound. Reprinted with permission from Bhargava and Feix (2004). Copyright 2004 by the Biophysical Society.

labeled antimicrobial peptide, CM15, in the presence and absence of liposomes (Bhargava and Feix, 2004). Under conditions where the peptide is membrane bound, the amplitude of the high-field ($m_I = -1$) line essentially disappears at the position of the aqueous signal. Consequently, the fraction of peptide remaining in the aqueous phase can be directly determined from the amplitude of the narrow line of the remaining free peptide, $A(-1)_f$, and the fraction of bound peptide is given by the reduction in signal amplitude as compared to a sample without membranes. Quantitatively, the fraction of bound peptide, f_b, is given by:

$$f_b = \left[\frac{A(-1)_f - A(-1)_x}{A(-1)_f - A(-1)_b}\right] \tag{10}$$

where $A(-1)_f$, $A(-1)_b$, and $A(-1)_x$ are the amplitudes of the high-field line for free peptide, fully bound peptide, and the experimental sample, respectively (Fig. 21). This method has been found to give comparable results to the more rigorous procedure of using spectral subtraction to separate the bound and free components and then integrating to determine the number of spins in each population (J.B.F., unpublished data). Once f_b has been determined at a series of lipid concentrations (where the peptide concentration is held constant), the molar partition coefficient (K_p) is calculated according to:

$$f_b = \frac{K_p[\text{lipid}]}{1 + K_p[\text{lipid}]} \tag{11}$$

and K_p can be used to calculate the change in free energy for membrane binding.

Results similar to those above have been described for a wide variety of peptide-membrane systems. Examples include binding of the ion-conductive peptide alamethicin (Archer *et al*., 1991; Lewis and Cafiso, 1999), a peptide derived from the effector domain of the myristoylated alanine-rich C-kinase substrate (Addona *et al*., 1997), a series of model peptides composed of lysine and phenylalanine and the spin-labeled amino acid tetramethylpiperidine-*N*-oxyl-4-amino-4-carboxylic acid (TOAC) (Victor and Cafiso, 2001), and the antimicrobial peptide cecropin AD (Mchaourab *et al*., 1994). Each of these systems gives EPR spectra quite similar to those in Fig. 21. Using a host–guest system of single amino acid substitutions into a spin-labeled, 25-residue peptide derived from yeast cytochrome *c* oxidase, Shin and coworkers used this approach to define a scale of relative membrane affinities for 14 uncharged amino acids (Thorgeirsson *et al*., 1996) and examined the thermodynamics of membrane partitioning (Russell *et al*., 1996). In addition, it should be noted that this method was first used to determine membrane surface potentials based on partitioning of spin-labeled amphiphiles (Cafiso and Hubbell, 1978; Castle and Hubbell, 1976), illustrating the generality of this approach.

2. Depth Measurements and Structure of the Membrane-Bound Peptide

Depth measurements based on CW saturation, as described earlier for integral membrane proteins, also can be used to determine the structure and penetration depths for membrane-associated peptides. Cysteine residues are introduced at various sites in the subject peptide, spin labeled, and their interaction with oxygen and NiEDDA (or other relaxation agent) determined under conditions where the peptide is fully membrane bound. Alternatively, if the peptide is being prepared by solid-phase peptide synthesis, labeling can be accomplished by introduction of the spin-labeled amino acid TOAC (e.g., Hanson *et al*., 1996; Karim *et al*., 2004; Marchetto *et al*., 1993; Victor and Cafiso, 2001). Since the TOAC nitroxide ring is rigidly incorporated into the α-carbon peptide backbone (Fig. 22), there are no internal side-chain fluctuations to be considered and the motion of the label directly reports on peptide backbone dynamics.

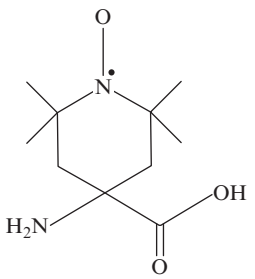

Fig. 22 The TOAC spin label can be integrated into the peptide backbone during synthesis.

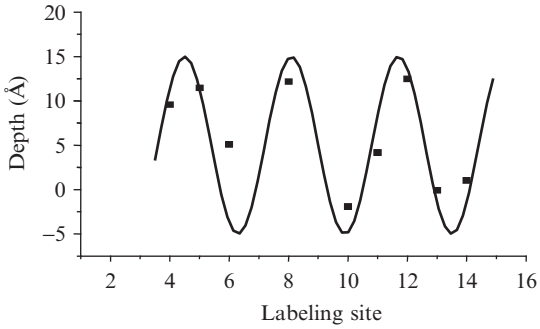

Fig. 23 Periodicity in depths for an α-helical peptide lying parallel to the membrane surface.

The peptides studied to date by SDSL have all been based on sequences with α-helical and/or random coil secondary structure. Such peptides can incorporate into the membrane with their helical axis parallel, perpendicular, or at an oblique angle relative to the bilayer surface, and all three cases have been observed experimentally. A nitroxide-scanning study of the antimicrobial peptide CM15 (Bhargava and Feix, 2004) indicated that this peptide was unstructured in solution, but upon membrane binding folded into an α-helix that aligned parallel to the bilayer surface, with the central axis of the helix located ~5 Å below the aqueous interface (Fig. 23). This is an essentially ideal location for membrane localization of this amphipathic peptide, allowing lysine residues on the polar face of the helix to "snorkel" out of the membrane and ion-pair with lipid phosphates while keeping hydrophobic residues on the nonpolar face of the helix buried in the hydrocarbon phase of the bilayer.

A 25-residue peptide containing the calmodulin-binding and protein kinase C-substrate domains of the MARCKS protein also aligned parallel to the membrane surface with a phenylalanine-rich region immersed ~8–10 Å below the lipid phosphates, but its highly charged N-terminal domain remained in the aqueous phase and it showed no evidence of helical structure when bound to membranes (Qin and Cafiso, 1996). When the phenylalanine residues of the native MARCKS-derived peptide were mutated to alanine, the peptide remained at the membrane surface, exposed to the aqueous phase—a shift of almost 15 Å in its equilibrium position (Victor *et al.*, 1999). This dramatic effect of phenylalanine residues on the immersion of the peptide was further investigated with model peptides containing only lysine and phenylalanine and the TOAC spin label (Victor and Cafiso, 2001). Again, replacement of two or more lysines with phenylalanine residues shifted the equilibrium position of the peptide by 13–15 Å, as determined by SDSL depth measurements.

Other peptides with sequences containing a mixture of polar and nonpolar amino acids have been found to insert into lipid bilayers at an angle relative to the membrane surface. This is a particularly predominant motif for peptides

involved in membrane fusion, such as peptides derived from SNARE proteins that function in vesicle trafficking (Xu *et al*., 2005) and viral fusion peptides (Han *et al*., 2001; Macosko *et al*., 1997). SDSL measurements on the amphipathic α-helical myelin basic protein determined an insertion angle of a mere 9° (Bates *et al*., 2004), while other peptides give much greater angles of insertion (Han *et al*., 2001; Macosko *et al*., 1997; Xu *et al*., 2005). In contrast, hydrophobic peptides, such as phospholamban (Karim *et al*., 2004), and a designed WALP peptide composed of a repeating leucine-alanine motif flanked by tryptophans (Nielsen *et al*., 2005) were shown to align in a vertical, transmembrane fashion, approximately perpendicular to the bilayer surface.

E. Unfolding and Kinetics

Denaturation studies, in which a protein is reversibly unfolded using either temperature or chemical denaturants [e.g., urea or guanidine hydrochloride (GdnHCl)], have been used extensively in recent years to examine protein structure and stability (see Chapter 11 by Street *et al*., this volume on protein folding). The sensitivity of the spin label EPR spectrum to the formation or loss of local structural constraints provides a highly sensitive means by which to monitor protein folding and denaturation, respectively. If a protein is labeled at a motionally restricted site, the loss of local tertiary structure that occurs upon denaturation will result in an increased spin label mobility and the corresponding appearance of a sharp, fast-motion component in the spectrum. Under conditions where there is an equilibrium between native and unfolded protein, the EPR spectrum will be a superposition of signals from the two populations and can be deconvoluted using spectral subtraction to determine the relative concentration of each component. In the case of a reversible, two-state denaturation, determination of the equilibrium distribution of folded and unfolded states as a function of denaturant concentration provides a direct measure of thermodynamic stability.

An example of the application of this technique using the ferric enterobactin receptor, FepA, is shown in Fig. 24. FepA was labeled at a site (E280C) known to have a strongly immobilized EPR spectrum in the native state and to be sensitive to ligand binding (Klug and Feix, 1998). Addition of either GdnHCl or urea resulted in the appearance of a rapid-motion component that increased in intensity with increasing denaturant concentration. The EPR spectrum of the fully denatured protein, obtained in 4 M GdnHCl, was used for spectral subtraction, and the fraction of denatured component was determined by integrating the spectra before and after subtraction. The difference spectra obtained after subtraction of the denatured component closely resembled the native spectrum, consistent with a two-state equilibrium between native and denatured states. Importantly, the spectrum reverted back to that of the native state upon removal of the denaturant by dialysis, demonstrating reversibility. Plots of the fraction of unfolded protein as a function of denaturant concentration provided additional evidence supporting a

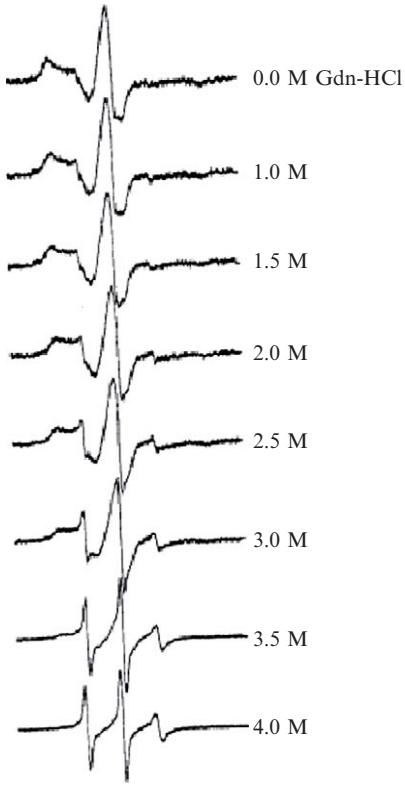

Fig. 24 Spectral changes in FepA at position 280 on addition of increasing amounts of GdnHCl denaturant. Reprinted with permission from Klug *et al.* (1995). Copyright 1995 American Chemical Society.

two-state equilibrium, giving estimates of the Gibbs free energy of unfolding and the stabilization provided by ligand binding (Klug and Feix, 1998).

It should be noted that protein denaturation studies done by SDSL measure very specifically the local unfolding at the site of the spin label. This can be very beneficial when studying a multidomain protein, as it allows the unfolding of each domain to be examined individually even in the intact protein, whereas other techniques that monitor global unfolding, such as circular dichroism, require the separate expression of each domain (Kim *et al.*, 2002). However, it must also be appreciated that different labeling sites may have different stabilities, as was observed in a subsequent study of FepA (Klug and Feix, 1998). Sequence-dependent differences in thermodynamic stability are also observed by NMR and mass spectrometry measurements of hydrogen–deuterium exchange and are an inherent aspect of protein structure.

Time-resolved EPR can be used to follow protein folding. In these studies an unfolded, spin-labeled protein in denaturant is mixed with buffer to rapidly dilute the denaturant concentration. Conversion of the narrow EPR lines of the denatured protein to the broader lines of the folded protein is observed by "sitting" on the peak of one of the sharp lines (i.e., by positioning the magnetic field at that resonance position and turning the magnetic field sweep off) and following the decrease in amplitude as a function of time. Using commercially available mixing cavities and syringe drives one can readily measure decays on the order of 0.1 sec. Scholes and coworkers, using cytochrome *c* as a model system, have developed and refined instrumentation allowing observation of kinetic components on the submillisecond timescale (DeWeerd *et al.*, 2001; Grigoryants *et al.*, 2000).

F. Distances to Determine Structural Arrangements and Monitor Dynamics

A number of outstanding studies have been carried out using EPR-determined distance measurements to examine tertiary folds, subunit interactions, and conformational changes (e.g., Altenbach *et al.*, 2001a,b; Berengian *et al.*, 1999; Brown *et al.*, 2002; Cordero-Morales *et al.*, 2006; Gross *et al.*, 1999; Koteiche *et al.*, 1998; Mchaourab *et al.*, 1997b; Wegener *et al.*, 2001). Three representative examples are described below.

1. Distance Measurements Using CW EPR

Distance measurements have been used extensively to examine light-induced conformational changes in the α-helical integral membrane protein rhodopsin (e.g., Altenbach *et al.*, 2001a,b; Cai *et al.*, 2001; Farrens *et al.*, 1996; Klein-Seetharaman *et al.*, 2001). Rhodopsin has long been used as a leading model system for the study of G–protein-coupled receptors (GPCRs). It contains seven transmembrane α-helices and a retinal chromophore that isomerizes upon photon absorption, triggering a conformational change that ultimately activates its cognate G-protein. In one of the earlier studies utilizing distance measurements to gain insights into changes in structure, five double-cysteine mutants were constructed—with one site on transmembrane helix 3 (TM3 or helix C) held constant and its interaction examined with five consecutive sites on TM6 (helix F) spanning a full turn of the helix (Farrens *et al.*, 1996). Samples were frozen after preparing the desired photochemical states at room temperature, and EPR spectra were obtained in the frozen state at 183 K. In the dark state, two of the spin label pairs were within ~12–14 Å, resulting in significantly broadened spectra, and the remaining three pairs were separated by distances in the range of 15–20 Å. After photoactivation, distances increased to greater than the 20 Å limit for detection of interaction for three of the spin label pairs, one pair became significantly closer, and one pair remained unchanged. These distance changes were the basis of a molecular model for photoactivation requiring TM6 to tilt away from the helical bundle

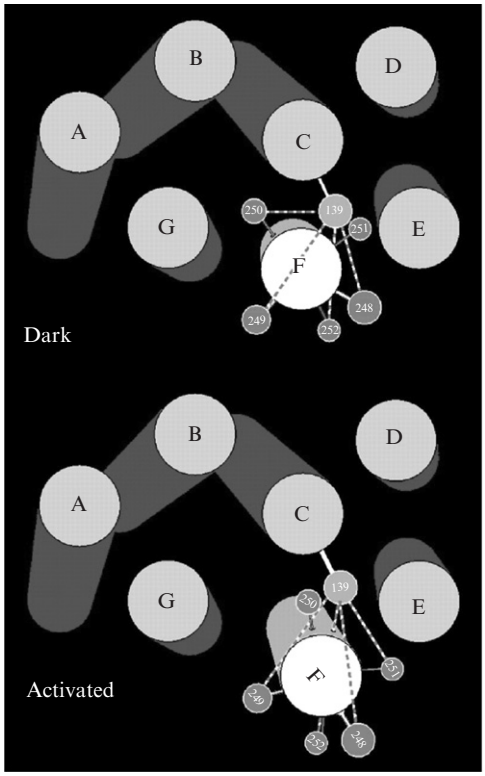

Fig. 25 Rhodopsin cartoon illustrating the conformational change in helix F that occurs upon light activation as elucidated using SDSL techniques. Reprinted with permission from Farrens *et al*. (1996). Copyright 1996 AAAS.

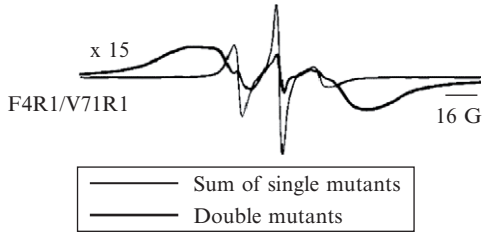

Fig. 26 Severe line broadening due to spin–spin interaction in T4L. Reprinted with permission from Mchaourab *et al*. (1997b). Copyright 1997 American Chemical Society.

(a displacement of ~8 Å) and to rotate (Farrens *et al*., 1996). This "tilt and rotate" model (Fig. 25) remains the current paradigm for activation of GPCRs.

An important goal in SDSL is to make interspin distance measurements on biomolecules in their native state, that is, in the liquid phase at ambient

temperature. In initial studies, T4L was used as a model system to develop methods to make such measurements (Mchaourab *et al.*, 1997b). The EPR spectra of double-labeled T4L mutants are compared to spectra obtained by taking the sum of the corresponding single mutant spectra. Pronounced broadening and distortion of line shapes are observed (e.g., Fig. 26). Note also that the line broadening is accompanied by a significant reduction in the amplitude of the double-labeled samples, as indicated by the increased gain used to display the spectrum. Since these studies were done at room temperature, it was possible to examine the effects of ligand binding on structure. Addition of a nonhydrolyzable substrate significantly increased spin–spin interaction for a number of pairs, consistent with a hinge-bending motion proposed as part of the mechanism for T4L catalysis (Mchaourab *et al.*, 1997b).

T4L was also used to develop methodology for deriving distances from room temperature spectra based on static dipolar coupling that can be extended to larger proteins (Altenbach *et al.*, 2001c). This interactive approach is based on Fourier deconvolution of dipolar-coupled spectra as introduced by Rabenstein and Shin (1995). A strength of this approach is the ability to determine distances even in the presence of singly labeled species. This is of particular importance, as for many systems it is often difficult to obtain stoichiometric labeling. A set of T4L double mutants was examined in frozen solution and at ambient temperature with sucrose added to decrease the tumbling rate of the protein. Noninteracting spectra were derived either from a sum of the singly labeled species or by labeling with a mixture of MTSL and a diamagnetic *N*-acetylated analogue. Good agreement was found between distances obtained at room temperature and in frozen solution, and in general it was found that residual motion of the spin label at ambient temperature had little effect on the estimated distances. In addition, distance distributions for a number of spin label pairs showed more than one maximum, consistent with the presence of multiple orientations of the spin label with respect to the peptide backbone as observed in crystal structures of MTSL-labeled T4L (Langen *et al.*, 2000).

2. Distance Measurements Using Pulse EPR

A comprehensive SDSL study on the solution structure of the cytoplasmic domain of the erythrocyte anion exchange protein, AE1 (also referred to as band 3) was carried out using a combination of CW EPR and DEER methodologies (Zhou *et al.*, 2005). The 42.5-kDa cytoplasmic domain of band 3 (cdb3) exists as a dimer that mediates numerous important protein–protein interactions with both soluble proteins (e.g., hemoglobin) and the erythrocyte cytoskeleton. A crystal structure of cdb3 obtained at pH 4.8 had shown an unexpectedly compact dimeric structure, but given the low pH used in crystallization, along with extensive evidence suggesting pH-dependent conformational changes, it was important to investigate the structure of cdb3 under more physiological conditions.

Recombinant expression, purification, and spin labeling of cdb3 mutants containing single-cysteine residues provided samples containing two spin labels per noncovalent dimer. Using SDSL, mobility and power saturation accessibility parameters confirmed the periodicity and expected accessibility for several elements of α-helical secondary structure observed in the crystal structure (Zhou *et al.*, 2005). One site in helix 10 (Q339R1) was particularly remarkable in that it displayed highly resolved dipolar coupling between the spin labels on each monomer. Simulation of the dipolar-coupled spectrum using a "tether-in-a-cone" model (Hustedt *et al.*, 2006) indicated an interspin distance of 14.7 ± 0.4 Å, in close agreement with the distance between these sites across the dimer interface inferred by the crystal structure. To further characterize the orientation of the two monomers in the cdb3 dimer, DEER was used to measure distances extending further out along helix 10 (from residues 340–345). Distances in the range 24.9–37.0 Å were measured (e.g., Fig. 14). The width of the distance distribution was very narrow (0.8–1.1 Å) for sites proximal to the core of dimer, and increased (3.6–6.6 Å) toward the distal end of the helix in a manner that paralleled the general increase in side-chain mobility. Distance measurements were also made for an additional 11 sites, using either DEER or by fitting CW EPR spectra with a Gaussian convolution model (Steinhoff *et al.*, 1997). Distances were reported in the range 6.2–47.7 Å, and again verified that the solution structure of cdb3 at neutral pH was in close agreement with the pH 4.8 crystal structure. Taken together, the data in this extensive study demonstrate the power of the SDSL approach in defining elements of local secondary structure and using distance measurements to elucidate how those secondary structure elements are arranged. The close agreement of the EPR data with that from the published crystal structure provides confidence that these methods can be used to determine unknown structures using SDSL alone.

III. Conclusion

As described and illustrated in this chapter, the SDSL EPR spectroscopy technique is able to address and answer questions often not solvable by genetic or crystal structure analysis. Its ability to analyze structure in a natural liquid-phase environment and its sensitivity to dynamics make the SDSL approach highly complementary to other structural methods. The number of researchers using SDSL techniques on their systems has grown tremendously in the past several years, and we look forward to future developments in methodology and new biological applications.

References

Addona, G. H., Andrews, S. H., and Cafiso, D. S. (1997). Estimating the electrostatic potential at the acetylcholine receptor agonist site using power saturation EPR. *Biochim. Biophys. Acta* **1329,** 74–84.

Altenbach, C., Cai, K., Klein-Seetharaman, J., Khorana, H. G., and Hubbell, W. L. (2001a). Structure and function in rhodopsin: Mapping light-dependent changes in distance between residue 65 in helix TM1 and residues in the sequence 306–319 at the cytoplasmic end of helix TM7 and in helix H8. *Biochemistry* **40,** 15483–15492.

Altenbach, C., Flitsch, S. L., Khorana, H. G., and Hubbell, W. L. (1989). Structural studies on transmembrane proteins. 2. Spin labeling of bacteriorhodopsin mutants at unique cysteines. *Biochemistry* **28,** 7806–7812.

Altenbach, C., Greenhalgh, D. A., Khorana, H. G., and Hubbell, W. L. (1994). A collision gradient method to determine the immersion depth of nitroxides in lipid bilayers: Application to spin-labeled mutants of bacteriorhodopsin. *Proc. Natl. Acad. Sci. USA* **91,** 1667–1671.

Altenbach, C., Klein-Seetharaman, J., Cai, K., Khorana, H. G., and Hubbell, W. L. (2001b). Structure and function in rhodopsin: Mapping light-dependent changes in distance between residue 316 in helix 8 and residues in the sequence 60–75, covering the cytoplasmic end of helices TM1 and TM2 and their connection loop CL1. *Biochemistry* **40,** 15493–15500.

Altenbach, C., Oh, K. J., Trabanino, R. J., Hideg, K., and Hubbell, W. L. (2001c). Estimation of inter-residue distances in spin labeled proteins at physiological temperatures: Experimental strategies and practical limitations. *Biochemistry* **40,** 15471–15482.

Archer, S. J., Ellena, J. F., and Cafiso, D. S. (1991). Dynamics and aggregation of the peptide ion channel alamethicin. Measurements using spin-labeled peptides. *Biophys. J.* **60,** 389–398.

Bates, I. R., Feix, J. B., Boggs, J. M., and Harauz, G. (2004). An immunodominant epitope of myelin basic protein is an amphipathic alpha-helix. *J. Biol. Chem.* **279,** 5757–5764.

Berengian, A. R., Parfenova, M., and Mchaourab, H. S. (1999). Site-directed spin labeling study of subunit interactions in the alpha-crystallin domain of small heat-shock proteins. Comparison of the oligomer symmetry in alphaA-crystallin, HSP 27, and HSP 16.3. *J. Biol. Chem.* **274,** 6305–6314.

Beth, A. H., Robinson, B. H., Cobb, C. E., Dalton, L. R., Trommer, W. E., Birktoft, J. J., and Park, J. H. (1984). Interactions and spatial arrangement of spin-labeled NAD + bound to glyceraldehyde-3-phosphate dehydrogenase. Comparison of EPR and X-ray modeling data. *J. Biol. Chem.* **259,** 9717–9728.

Bhargava, K., and Feix, J. B. (2004). Membrane binding, structure, and localization of Cecropin-Mellitin hybrid peptides: A site-directed spin-labeling study. *Biophys. J.* **86,** 329–336.

Bonora, M., Becker, J., and Saxena, S. (2004). Suppression of electron spin-echo envelope modulation peaks in double quantum coherence electron spin resonance. *J. Magn. Reson.* **170,** 278–283.

Borbat, P. P., Costa-Filho, A. J., Earle, K. A., Moscicki, J. K., and Freed, J. H. (2001). Electron spin resonance in studies of membranes and proteins. *Science* **291,** 266–269.

Borbat, P. P., and Freed, J. H. (2000). Double-Quantum ESR and distance measurements. *In* "Biological Magnetic Resonance" (L. J. Berliner, S. S. Eaton, and G. R. Eaton, eds.), pp. 383–459. Kluwer Academic/Plenum Publishers, New York.

Borbat, P. P., Mchaourab, H. S., and Freed, J. H. (2002). Protein structure determination using long-distance constraints from double-quantum coherence ESR: Study of T4 lysozyme. *J. Am. Chem. Soc.* **124,** 5304–5314.

Brown, L. J., Sale, K. L., Hills, R., Rouviere, C., Song, L., Zhang, X., and Fajer, P. G. (2002). Structure of the inhibitory region of troponin by site directed spin labeling electron paramagnetic resonance. *Proc. Natl. Acad. Sci. USA* **99,** 12765–12770.

Buchaklian, A. H., and Klug, C. S. (2005). Characterization of the Walker A motif of MsbA using site-directed spin labeling electron paramagnetic resonance spectroscopy. *Biochemistry* **44,** 5503–5509.

Buchanan, S. K., Smith, B. S., Venkatramani, L., Xia, D., Esser, L., Palnitkar, M., Chakraborty, R., van der, H. D., and Deisenhofer, J. (1999). Crystal structure of the outer membrane active transporter FepA from Escherichia coli. *Nat. Struct. Biol.* **6,** 56–63.

Budil, D. E., Lee, S., Saxena, S., and Freed, J. H. (1996). Nonlinear-least-squares analysis of slow-motion EPR spectra in one and two dimensions using a modified Levenberg-Marquardt Algorithm. *J. Magn. Reson.* **120,** 155–189.

Cafiso, D. S., and Hubbell, W. L. (1978). Estimation of transmembrane pH gradients from phase equilibria of spin-labeled amines. *Biochemistry* **17,** 3871–3877.

Cai, K., Klein-Seetharaman, J., Altenbach, C., Hubbell, W. L., and Khorana, H. G. (2001). Probing the dark state tertiary structure in the cytoplasmic domain of rhodopsin: Proximities between amino acids deduced from spontaneous disulfide bond formation between cysteine pairs engineered in cytoplasmic loops 1, 3, and 4. *Biochemistry* **40,** 12479–12485.

Castle, J. D., and Hubbell, W. L. (1976). Estimation of membrane surface potential and charge density from the phase equilibrium of a paramagnetic amphiphile. *Biochemistry* **15,** 4818–4831.

Columbus, L., and Hubbell, W. L. (2002). A new spin on protein dynamics. *Trends Biochem. Sci.* **27,** 288–295.

Columbus, L., and Hubbell, W. L. (2004). Mapping backbone dynamics in solution with site-directed spin labeling: GCN4–58 bZip free and bound to DNA. *Biochemistry* **43,** 7273–7287.

Columbus, L., Kalai, T., Jeko, J., Hideg, K., and Hubbell, W. L. (2001). Molecular motion of spin labeled side chains in alpha-helices: Analysis by variation of side chain structure. *Biochemistry* **40,** 3828–3846.

Cordero-Morales, J. F., Cuello, L. G., Zhao, Y., Jogini, V., Cortes, D. M., Roux, B., and Perozo, E. (2006). Molecular determinants of gating at the potassium-channel selectivity filter. *Nat. Struct. Mol. Biol.* **13,** 311–318.

Dalton, L. A., McIntyre, J. O., and Flewelling, R. F. (1987). Distance estimate of the active center of D-β-hydroxybutyrate dehydrogenase from the membrane surface. *Biochemistry* **26,** 2117–2130.

DeWeerd, K., Grigoryants, V. M., Sun, Y., Fetrow, J. S., and Scholes, C. P. (2001). EPR-detected folding kinetics of externally located Cysteine-directed spin-labeled mutants of Iso-1-cytochrome *c*. *Biochemistry* **40,** 15846–15855.

Eaton, G. R., Eaton, S. S., and Berliner, L. J. (eds.) (2000). Distance Measurements in Biological Systems by EPR "Biological Magnetic Resonance," Vol. 19. Kluwer, New York.

Fajer, P. G. (2000). Electron spin resonance spectroscopy labeling in peptide and protein analysis. *In* "Encyclopedia of Analytical Chemistry" (R. A. Meyers, ed.), pp. 5725–5761. John Wiley and Sons Ltd., Chichester.

Farrens, D. L., Altenbach, C., Yang, K., Hubbell, W. L., and Khorana, H. G. (1996). Requirement of rigid-body motion of transmembrane helices for light activation of rhodopsin. *Science* **274,** 768–770.

Feix, J. B., and Klug, C. S. (1998). Site-directed spin labeling of membrane proteins and peptide-membrane interactions. *In* "Biological Magnetic Resonance, Volume 14: Spin Labeling: The Next Millennium" (L. J. Berliner, ed.), pp. 252–281. Plenum Press, New York.

Freed, J. H. (2000). New technologies in electron spin resonance. *Annu. Rev. Phys. Chem.* **51,** 655–689.

Gaffney, B. J. (1976). Practical considerations for the calculation of order parameters. *In* "Spin Labeling: Theory and Applications" (L. J. Berliner, ed.), pp. 567–571. Academic Press, New York.

Griffith, O. H., and Jost, P. C. (1976). Lipid spin labels in biological membranes. *In* "Spin Labeling: Theory and Applications" (L. J. Berliner, ed.), pp. 453–523. Academic Press, New York.

Grigoryants, V. M., Veselov, A. V., and Scholes, C. P. (2000). Variable velocity liquid flow EPR applied to submillisecond protein folding. *Biophys. J.* **78,** 2702–2708.

Gross, A., Columbus, L., Hideg, K., Altenbach, C., and Hubbell, W. L. (1999). Structure of the KcsA potassium channel from Streptomyces lividans: A site-directed spin labeling study of the second transmembrane segment. *Biochemistry* **38,** 10324–10335.

Han, X., Bushweller, J. H., Cafiso, D. S., and Tamm, L. K. (2001). Membrane structure and fusion-triggering conformational change of the fusion domain from influenza hemagglutinin. *Nat. Struct. Biol.* **8,** 715–720.

Hanson, P., Millhauser, G., Formaggio, F., Crisma, M., and Toniolo, C. (1996). ESR characterization of hexameric, helical peptides using double TOAC spin labeling. *J. Am. Chem. Soc.* **118,** 7618–7625.

Hanson, S. M., Francis, D. J., Vishnivetskiy, S. A., Kolobova, E. A., Hubbell, W. L., Klug, C. S., and Gurevich, V. V. (2006). Differential interaction of spin-labeled arrestin with inactive and active phosphorhodopsin. *Proc. Natl. Acad. Sci. USA* **103,** 4900–4905.

Hubbell, W. L., Cafiso, D. S., and Altenbach, C. (2000). Identifying conformational changes with site-directed spin labeling. *Nat. Struct. Biol.* **7,** 735–739.

Hubbell, W. L., Gross, A., Langen, R., and Lietzow, M. A. (1998). Recent advances in site-directed spin labeling of proteins. *Curr. Opin. Struct. Biol.* **8,** 649–656.

Hubbell, W. L., and McConnell, H. M. (1968). Spin-label studies of the excitable membranes of nerve and muscle. *Proc. Natl. Acad. Sci. USA* **61,** 12–16.

Hubbell, W. L., Mchaourab, H. S., Altenbach, C., and Lietzow, M. A. (1996). Watching proteins move using site-directed spin labeling. *Structure* **4,** 779–783.

Hustedt, E. J., and Beth, A. H. (1999). Nitroxide spin-spin interactions: Applications to protein structure and dynamics. *Annu. Rev. Biophys. Biomol. Struct.* **28,** 129–153.

Hustedt, E. J., and Beth, A. H. (2000). Structural information from CW-EPR spectra of dipolar coupled nitroxide spin labels. *In* "Biological Magnetic Resonance" (L. J. Berliner, S. S. Eaton, and G. R. Eaton, eds.), pp. 155–184. Kluwer Academic/Plenum Publishers, New York.

Hustedt, E. J., Smirnov, A. I., Laub, C. F., Cobb, C. E., and Beth, A. H. (1997). Molecular distances from dipolar coupled spin-labels: The global analysis of multifrequency continuous wave electron paramagnetic resonance data. *Biophys. J.* **72,** 1861–1877.

Hustedt, E. J., Stein, R. A., Sethaphong, L., Brandon, S., Zhou, Z., and Desensi, S. C. (2006). Dipolar coupling between nitroxide spin labels: The development and application of a tether-in-a-cone model. *Biophys. J.* **90,** 340–356.

Isas, J. M., Langen, R., Haigler, H. T., and Hubbell, W. L. (2002). Structure and dynamics of a helical hairpin and loop region in annexin 12: A site-directed spin labeling study. *Biochemistry* **41,** 1464–1473.

Jao, C. C., Der-Sarkissian, A., Chen, J., and Langen, R. (2004). Structure of membrane-bound alpha-synuclein studied by site-directed spin labeling. *Proc. Natl. Acad. Sci. USA* **101,** 8331–8336.

Karim, C. B., Kirby, T. L., Zhang, Z., Nesmelov, Y., and Thomas, D. D. (2004). Phospholamban structural dynamics in lipid bilayers probed by a spin label rigidly coupled to the peptide backbone. *Proc. Natl. Acad. Sci. USA* **101,** 14437–14442.

Karim, C. B., Stamm, J. D., Karim, J., Jones, L. R., and Thomas, D. D. (1998). Cysteine reactivity and oligomeric structures of phospholamban and its mutants. *Biochemistry* **37,** 12074–12081.

Kim, C. S., Kweon, D. H., and Shin, Y. K. (2002). Membrane topologies of neuronal SNARE folding intermediates. *Biochemistry* **41,** 10928–10933.

Klein-Seetharaman, J., Hwa, J., Cai, K., Altenbach, C., Hubbell, W. L., and Khorana, H. G. (2001). Probing the dark state tertiary structure in the cytoplasmic domain of rhodopsin: Proximities between amino acids deduced from spontaneous disulfide bond formation between Cys316 and engineered cysteines in cytoplasmic loop 1. *Biochemistry* **40,** 12472–12478.

Klug, C. S., Eaton, S. S., Eaton, G. R., and Feix, J. B. (1998). Ligand-induced conformational change in the ferric enterobactin receptor FepA as studied by site-directed spin labeling and time-domain ESR. *Biochemistry* **37,** 9016–9023.

Klug, C. S., and Feix, J. B. (1998). Guanidine hydrochloride unfolding of a transmembrane beta-strand in FepA using site-directed spin labeling. *Protein Sci.* **7,** 1469–1476.

Klug, C. S., and Feix, J. B. (2004). SDSL: A survey of biological applications. *In* "Biological Magnetic Resonance" (L. J. Berliner, S. S. Eaton, and G. R. Eaton, eds.), Vol. 24, pp. 269–308. Kluwer Academic/Plenum Publishers, Hingham, MA.

Klug, C. S., Su, W., and Feix, J. B. (1997). Mapping of the residues involved in a proposed beta-strand located in the ferric enterobactin receptor FepA using site-directed spin-labeling. *Biochemistry* **36,** 13027–13033.

Klug, C. S., Su, W., Liu, J., Klebba, P. E., and Feix, J. B. (1995). Denaturant unfolding of the ferric enterobactin receptor and ligand-induced stabilization studied by site-directed spin labeling. *Biochemistry* **34,** 14230–14236.

Koteiche, H. A., Berengian, A. R., and Mchaourab, H. S. (1998). Identification of protein folding patterns using site-directed spin labeling. Structural characterization of a beta-sheet and putative substrate binding regions in the conserved domain of alpha A-crystallin. *Biochemistry* **37,** 12681–12688.

Langen, R., Isas, J. M., Luecke, H., Haigler, H. T., and Hubbell, W. L. (1998). Membrane-mediated assembly of annexins studied by site-directed spin labeling. *J. Biol. Chem.* **273,** 22453–22457.

Langen, R., Oh, K. J., Cascio, D., and Hubbell, W. L. (2000). Crystal structures of spin labeled T4 lysozyme mutants: Implications for the interpretation of EPR spectra in terms of structure. *Biochemistry* **39,** 8396–8405.

Lewis, J. R., and Cafiso, D. S. (1999). Correlation between the free energy of a channel-forming voltage-gated peptide and the spontaneous curvature of bilayer lipids. *Biochemistry* **38,** 5932–5938.

Lietzow, M. A., and Hubbell, W. L. (1998). Site-directed spin labeling of cellular retinol-binding protein (CRBP): Examination of a β-sheet landscape and its conformational dynamics. *Biophys. J.* **74**(2), A278.

Lietzow, M. A., and Hubbell, W. L. (2004). Motion of spin label side chains in cellular retinol-binding protein: Correlation with structure and nearest-neighbor interactions in an antiparallel β-sheet. *Biochemistry* **43,** 3137–3151.

Macosko, J. C., Kim, C. H., and Shin, Y. K. (1997). The membrane topology of the fusion peptide region of influenza hemagglutinin determined by spin-labeling EPR. *J. Mol. Biol.* **267,** 1139–1148.

Marchetto, R., Schreier, S., and Nakaie, C. R. (1993). A novel spin-labeled amino acid derivative for use in peptide synthesis: (9-Fluorenylmethyloxycarbonyl)-2,2,6,6-tetramethylpiperidine-N-oxyl-4-amino-carboxylic acid. *J. Am. Chem. Soc.* **115,** 11042–11043.

Marsh, D. (2001). Polarity and permeation profiles in lipid membranes. *Proc. Natl. Acad. Sci. USA* **98,** 7777–7782.

Mchaourab, H. S., Berengian, A. R., and Koteiche, H. A. (1997a). Site-directed spin-labeling study of the structure and subunit interactions along a conserved sequence in the alpha-crystallin domain of heat-shock protein 27. Evidence of a conserved subunit interface. *Biochemistry* **36,** 14627–14634.

Mchaourab, H. S., Hyde, J. S., and Feix, J. B. (1994). Binding and state of aggregation of spin-labeled cecropin AD in phospholipid bilayers: Effects of surface charge and fatty acyl chain length. *Biochemistry* **33,** 6691–6699.

Mchaourab, H. S., Oh, K. J., Fang, C. J., and Hubbell, W. L. (1997b). Conformation of T4 lysozyme in solution. Hinge-bending motion and the substrate-induced conformational transition studied by site-directed spin labeling. *Biochemistry* **36,** 307–316.

Merianos, H. J., Cadieux, N., Lin, C. H., Kadner, R. J., and Cafiso, D. S. (2000). Substrate-induced exposure of an energy-coupling motif of a membrane transporter. *Nat. Struct. Biol.* **7,** 205–209.

Millhauser, G. L. (1992). Selective placement of electron spin resonance spin labels: New structural methods for peptides and proteins. *Trends Biochem. Sci.* **17,** 448–452.

Nielsen, R. D., Che, K., Gelb, M. H., and Robinson, B. H. (2005). A ruler for determining the position of proteins in membranes. *J. Am. Chem. Soc.* **127,** 6430–6442.

Palmer, A. G., III. (2001). Nmr probes of molecular dynamics: Overview and comparison with other techniques. *Annu. Rev. Biophys. Biomol. Struct.* **30,** 129–155.

Pannier, M., Veit, S., Godt, A., Jeschke, G., and Spiess, H. W. (2000). Dead-time free measurement of dipole-dipole interactions between electron spins. *J. Magn. Reson.* **142,** 331–340.

Perozo, E., Cortes, D. M., and Cuello, L. G. (1998). Three-dimensional architecture and gating mechanism of a K+ channel studied by EPR spectroscopy. *Nat. Struct. Biol.* **5,** 459–469.

Perozo, E., Cortes, D. M., Sompornpisut, P., Kloda, A., and Martinac, B. (2002). Open channel structure of MscL and the gating mechanism of mechanosensitive channels. *Nature* **418,** 942–948.

Perozo, E., Kloda, A., Cortes, D. M., and Martinac, B. (2001). Site-directed spin-labeling analysis of reconstituted Mscl in the closed state. *J. Gen. Physiol.* **118,** 193–206.

Qin, Z., and Cafiso, D. S. (1996). Membrane structure of protein kinase C and calmodulin binding domain of myristoylated alanine rich C kinase substrate determined by site-directed spin labeling. *Biochemistry* **35,** 2917–2925.

Rabenstein, M. D., and Shin, Y. K. (1995). Determination of the distance between two spin labels attached to a macromolecule. *Proc. Natl. Acad. Sci. USA* **92,** 8239–8243.

Russell, C. J., Thorgeirsson, T. E., and Shin, Y. K. (1996). Temperature dependence of polypeptide partitioning between water and phospholipid bilayers. *Biochemistry* **35,** 9526–9532.

Steinhoff, H. J., Radzwill, N., Thevis, W., Lenz, V., Brandenburg, D., Antson, A., Dodson, G., and Wollmer, A. (1997). Determination of interspin distances between spin labels attached to insulin: Comparison of electron paramagnetic resonance data with the X-ray structure. *Biophys. J.* **73,** 3287–3298.

Stone, T. J., Buckman, T., Nordio, P. L., and McConnell, H. M. (1965). Spin-labeled biomolecules. *Proc. Natl. Acad. Sci. USA* **54,** 1010–1017.

Thompson, L. V., Lowe, D. A., Ferrington, D. A., and Thomas, D. D. (2001). Electron paramagnetic resonance: A high-resolution tool for muscle physiology. *Exerc. Sport Sci. Rev.* **29,** 3–6.

Thorgeirsson, T. E., Russell, C. J., King, D. S., and Shin, Y. K. (1996). Direct determination of the membrane affinities of individual amino acids. *Biochemistry* **35,** 1803–1809.

Victor, K., Jacob, J., and Cafiso, D. S. (1999). Interactions controlling the membrane binding of basic protein domains: Phenylalanine and the attachment of the myristoylated alanine-rich C-kinase substrate protein to interfaces. *Biochemistry* **38,** 12527–12536.

Victor, K. G., and Cafiso, D. S. (2001). Location and dynamics of basic peptides at the membrane interface: Electron paramagnetic resonance spectroscopy of tetramethyl-piperidine-N-oxyl-4-amino-4-carboxylic acid-labeled peptides. *Biophys. J.* **81,** 2241–2250.

Voss, J., He, M. M., Hubbell, W. L., and Kaback, H. R. (1996). Site-directed spin labeling demonstrates that transmembrane domain XII in the lactose permease of Escherichia coli is an alpha-helix. *Biochemistry* **35,** 12915–12918.

Wegener, A. A., Klare, J. P., Engelhard, M., and Steinhoff, H. J. (2001). Structural insights into the early steps of receptor-transducer signal transfer in archaeal phototaxis. *EMBO J.* **20,** 5312–5319.

Xiao, W., and Shin, Y. K. (2000). EPR spectroscopic ruler: The method and its applications. *In* "Biological Magnetic Resonance" (L. J. Berliner, S. S. Eaton, and G. R. Eaton, eds.), Vol. 19, pp. 249–276. Kluwer Academic/Plenum Publishers, New York.

Xu, Y., Zhang, F., Su, Z., McNew, J. A., and Shin, Y. K. (2005). Hemifusion in SNARE-mediated membrane fusion. *Nat. Struct. Mol. Biol.* **12,** 417–422.

Yang, K., Farrens, D. L., Altenbach, C., Farahbakhsh, Z. T., Hubbell, W. L., and Khorana, H. G. (1996). Structure and function in rhodopsin. Cysteines 65 and 316 are in proximity in a rhodopsin mutant as indicated by disulfide formation and interactions between attached spin labels. *Biochemistry* **35,** 14040–14046.

Yu, Y. G., Thorgeirsson, T. E., and Shin, Y. K. (1994). Topology of an amphiphilic mitochondrial signal sequence in the membrane-inserted state: A spin labeling study. *Biochemistry* **33,** 14221–14226.

Zhang, Y., and Shin, Y. K. (2006). Transmembrane organization of yeast syntaxin-analogue Sso1p. *Biochemistry* **45,** 4173–4181.

Zhao, M., Zen, K. C., Hernandez-Borrell, J., Altenbach, C., Hubbell, W. L., and Kaback, H. R. (1999). Nitroxide scanning electron paramagnetic resonance of helices IV and V and the intervening loop in the lactose permease of Escherichia coli. *Biochemistry* **38,** 15970–15977.

Zhou, Z., Desensi, S. C., Stein, R. A., Brandon, S., Dixit, M., McArdle, E. J., Warren, E. M., Kroh, H. K., Song, L., Cobb, C. E., Hustedt, E. J., and Beth, A. H. (2005). Solution structure of the cytoplasmic domain of erythrocyte membrane band 3 determined by site-directed spin labeling. *Biochemistry* **44,** 15115–15128.